Formation and growth of diapirs in contractional settings: the Mediano anticline and Clamosa diapir case study (Southern Pyrenees)

Pablo Santolaria[1], Roi Silva-Casal[1], Núria Carrera[1], Josep A. Muñoz[1], Pau Arbués[1], Pablo Granado[1]

[1]Institut de Recerca Geomodels, Departament de Dinàmica de la Terra i de L'Oceà, Universitat de Barcelona (UB), C/Martí i Franquès s/n 08028 Barcelona, Spain.

Correspondence to: Pablo Santolaria (p.santolaria.otin@ub.edu)

Abstract. At the northwestern termination of the South Pyrenean Central Salient, thrust imbrication, detachment folding and diapirism are structurally and genetically related. The La Fueba imbricate system has been folded by the Mediano detachment anticline, while this fold connects with the Clamosa diapir. Together, this structural-stratigraphic trinity provides an excellent example to evaluate the factors controlling purely contractional diapirs in onshore-offshore contractional fold-thrust systems. Our study integrates detailed geological mapping, a large structural dataset, new biostratigraphic data, and interpretations of well-tied depth-converted seismic lines and cross-sections. A combined evolutionary model for contractional ~~diapir~~diapirs formation and evolution is presented. While less common than in extensional settings, the interplay of shortening of a salt horizon along with vertical axis rotations and local stretching and erosion of the overburden can lead to purely contractional salt diapirs.

1 Introduction

Salt-detached fold-and-thrust belts feature a common structural style characterized by low taper angles and regularly-spaced folds and thrusts (Davis and Engelder, 1985). Folds are usually symmetrical, upright, elongated, and display a regular wavelength (e.g., Davis and Engelder, 1985; Harrison, 1995; Rowan and Vendeville, 2006). Salt thickness is a primary factor in determining the type of fold: a thicker salt than its overburden promotes the formation of salt-cored detachment folds, whereas thinner salt leads to thrusted folds (Stewart, 1999). Besides, the ratio of décollement thickness to cover thickness and the décollement strength (i.e., viscosity) control the structural spacing, fold amplitude, wavelength, and structural facing (e.g. Cotton and Koyi, 2000; Costa and Vendeville, 2002; Soto et al., 2002; Ruh et al., 2012). On the other hand, sedimentation-erosion processes localize deformation and promote fold amplification (e.g. Storti and McClay, 1995; Mugnier et al., 1997; Pichot and Nalpas, 2009; Fillon et al., 2013; Duerto and McClay, 2009; Izquierdo-Llavall et al., 2018; Pla et al., 2019). ~~It must be borne in mind that~~All these factors can vary both spatially and temporally, and so may the associated structural styles and kinematics.

Many salt-detached fold-and-thrust belts include salt diapirs, such as in the Fars province area in the Zagros fold-belt (e.g. Jahani et al., 2009; Callot et al., 2012; Snidero et al., 2020), the Hellenides (e.g., Velaj et al., 2002; Vakalas et al., 2023), the

SW Sub-Alpine chains (e.g. Célini et al., 2020), the Atlas Mountains (e.g. Saura et al., 2014; Teixell et al., 2017; Calvín et al., 2018; Martín-Martín, 2017; Casas-Sainz et al., 2023), the Betic Cordillera (e.g. De Ruig, 1995; Roca et al., 2006; Escosa et al., 2018; Flinch and Soto, 2022) and the Pyrenees (e.g. Canérot et al., 2005; Muñoz et al., 2013; Santolaria et al., 2016; Burrel and Teixell, 2021; Cassini et al., 2023), among others. In most cases, diapirs in such settings are inherited features, originating from extension, differential loading, or gravitational gliding on rifted margins predating contraction (e.g. Roca et al., 2006; Santolaria et200et al., 2022; Strauss et al., 2023). Upon shortening and due to the low-strength of salt, diapirs are easily rejuvenated (e.g. Vendeville and Nilsen, 1995; Callot et al., 2012; Dooley et al., 2009; Granado et al. 2019; Santolaria et al., 2021a) and commonly focus deformation and localize contractional structures (e.g. Rowan and Vendeville, 2006; Santolaria et al., 2021b). In the absence of inherited salt structures, diapirism in fold-and-thrust belts is less common (Vendeville and Jackson, 1992; Jackson and Vendeville, 1994) and is hindered by factors such as: i) a relatively thick cover strengthened by horizontal contractional stresses, ii) a relatively thin décollement (i.e., the salt budget limiting factor), iii) predominance of thrusting over folding, and iv) high syn-contractional sedimentary rates (Bonini, 2003; Barrier et al., 2013) (Fig. 1a). Therefore, triggers and processes that enhance diapirism in such settings include: i) a relatively thin cover over a thick salt décollement, ii) folding rather than thrusting, iii) low to moderate syn-contractional sedimentary rate relative to uplift, thus favouring erosion (Sans and Koyi, 2001), v) lateral gradients of thrust displacement accommodated with localized extension, vi) salt migration and inflation (Fig. 1b), vii) the presence of salt in the hanging wall of a thrust carried up to shallow levels where it can break through to the surface (Rowan, 2020), viii) salt breaking through the thin roof of an early salt-cored anticline or the thick roof of a later fold that is thinned by erosion (Coward & Stewart, 1995).

What are then the feedbacks and necessary balance between unfavourable and favourable factors critical for the occurrence of diapirism and its subsequent enhancement or inhibition?
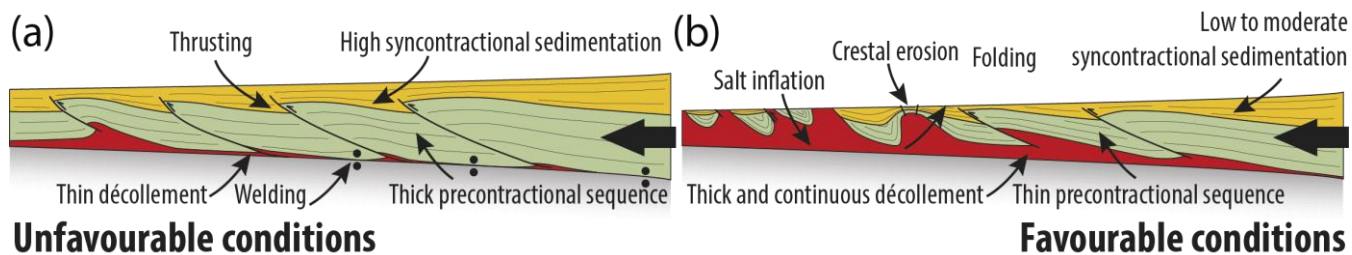
Figure 1: Summary sketches that illustrate unfavorable (A) and favorable (B) conditions for the development of purely contractional diapirs in fold-and-thrust belts.

In this contribution, we present the South Pyrenean Central Salient as a unique scenario due to the outstanding preservation of syn-contractional growth strata and the available subsurface data surrounding several salt bodies. Our analysis assesses the feedbacks and balance between diapirism triggers and inhibiting factors and processes (e.g., Muñoz et al., 2024). We illustrate these dynamics trough through a detailed case study of the Clamosa diapir, a Triassic salt body surrounded by pre-, syn-, and

post-tectonic units (Fig. 2), along with nearby contractional structures: the Mediano detachment anticline, and the La Fueba imbricate thrust system. Our methodology included constructing a detailed new geological map completed based on our own fieldwork and the synthesis of previous geological maps (Arbués ~~and Corregidor, 1995; Arbués~~ et al., 2007; Fernández et al., 2004; Teixell and Barnolas, 1995; Gomis et al., 2012; Garrido-Megías, 1973; Poblet et al., 1998; ~~Barnolas~~Teixell et al., 1994b).

65 This surface geology work is complemented by constructing and analysing serial cross-sections integrated with and supported by well-tied depth-converted 2D seismic data. In addition, our structural-kinematic evolutionary model is supported by new biostratigraphy dating based on foraminifera content from key localities. Our proposed model is framed within the regional context of the South Pyrenean Central Salient (Muñoz et al., 2018, 2024). Additionally, we evaluate and discuss the factors that determine the formation of salt diapirs in fold-and-thrust belts, and their connection with adjacent non-diapiric structures,

70 such as detachment anticlines and thrust imbricates.

2. Geological setting

2.1. The South-Central Pyrenees

75

The Pyrenean mountain range formed as a result of the collision between the Eurasian and Iberian plates from Late Cretaceous to Miocene times~~, resulting in the growth of an asymmetric doubly vergent orogenic wedge~~ (Roest and Srivastava, 1991; Rosenbaum et al., 2002). This collision involved the subduction of the Iberian lower crust attached to its lithospheric mantle beneath the European Plate resulting in the growth of an asymmetric doubly-verging orogenic wedge (Choukroune, 1989;

80 Muñoz, 1992; Pedreira et al., 2003; Campanyà et al., 2012; Chevrot et al., 2015, 2018), ~~and~~together with the inversion of the Late Jurassic-Early Cretaceous rifted margin (Mencós et al. 2015; Muñoz et al. 2018). The Pyrenean structural style is thus mainly controlled by the inversion of inherited features but also by the distribution of the Triassic evaporites and shales, which acted as the regional thin-skinned décollement in the Southern Pyrenees. The South-Central Pyrenees form a thrust salient (Fig. 2) whose curvature developed by the progressive bending resulting from divergent thrust transport directions (Muñoz et

85 al., 2013; 2024). Preservation of syntectonic sediments since the early stages of convergence provides constraints on the thrusts' sheets kinematics of the salient. From north to south, and older to younger, these thrust sheets are: the Late Cretaceous Cotiella-Bóixols, the Paleocene-late Ypresian Peña Montañesa-Montsec, and the Lutetian-Oligocene Gavarnie-Sierras thrust sheets. Displacement of these thrust sheets was coeval with basement-involved thrusting in the Axial Zone (Séguret, 1972; Cámara and Klimowitz, 1985). In the Gavarnie-Sierras thrust sheet displacement is mainly accounted by several basement-

90 involved thrusts, such as the Gavarnie, Bielsa and Guarga thrusts that mostly moved diachronously and in sequence (Séguret, 1972; Cámara and Klimowitz, 1985; Martínez-Peña and Casas-Sainz, 2003). The Gavarnie thrust started to develop during early Lutetian times (the age of the onset of folding in its hanging wall, Séguret, 1972; Fernández et al., 2012; Muñoz et al., 2013), until it was tilted, folded, and piggy-back transported southwards since late Eocene times by the Guarga and related basement thrusts.
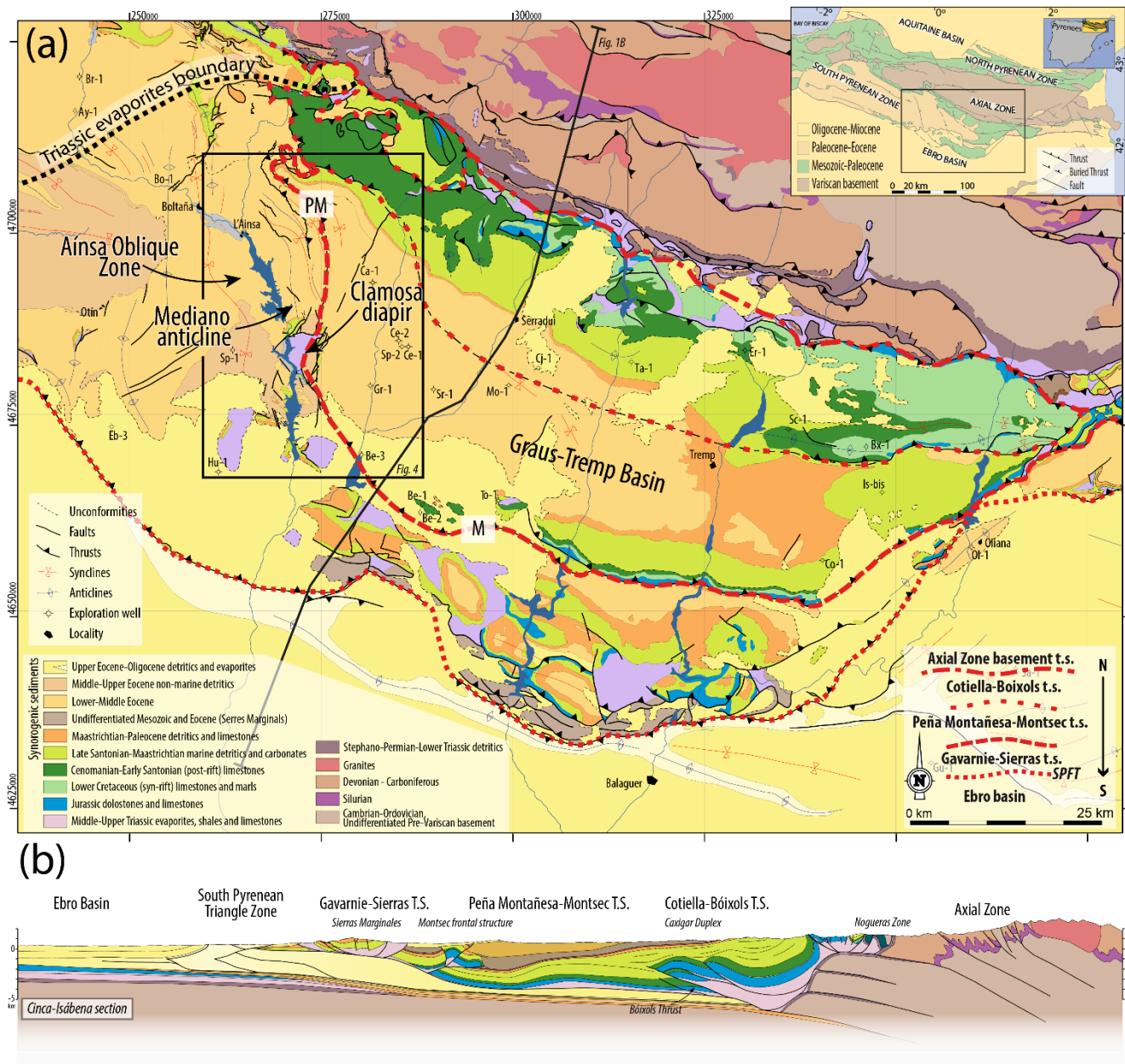
Figure 2. (a), Geological map of the South Pyrenean Central Salient. Dashed and dotted red lines represent the contact between the Axial Zone and the Southern Pyrenean fold and thrust belts and the Bóixols-Cotiella, Montsec-Peña Montañesa and Gavarnie-Sierras thrust sheets (modified from Muñoz et al., 2018 and Santolaria et al., 2024; inset map after Beamud, 2013). A black rectangle

frames the studied area shown in Fig. 4. (b), Cross-section illustrates the western half of this Pyrenean Salient (from Santolaria et al., 2024). PM, Peña Montañesa thrust; M, Montsec thrust.
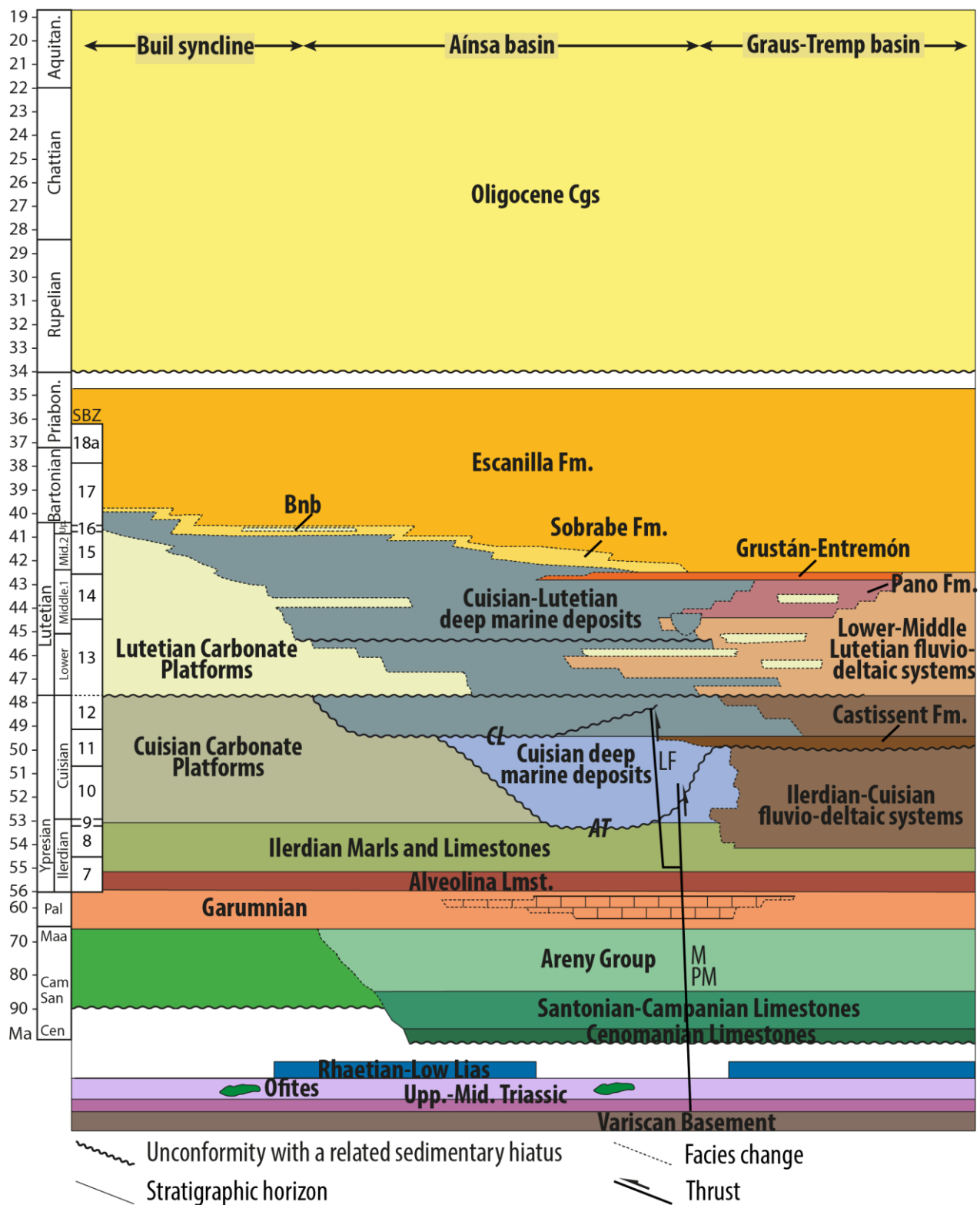
The studied area is on the western edge of the South Pyrenean Central Salient, where the N130E trending Montsec thrust turns into a N-S orientation to merge with the Peña Montañesa south-directed thrust system (Fig. 2). East of it, the Graus-Tremp basin extends to the east as the piggyback basin ridding on top of the Montsec thrust sheet (Fig. 2). West of it, the Mediano anticline and Clamosa diapir are the easternmost structures of a set of N-S trending folds that belong to the Aínsa Oblique Zone (Muñoz et al., 2013). Besides, the Clamosa diapir represents the northernmost diapir of those structures belonging to the Gavarnie-Sierras thrust sheet. Paleomagnetic and structural studies have revealed the N-S folds in the Gavarnie-Sierras thrust sheet originated slightly oblique to the Pyrenean main N120E trend and underwent syn- to post-folding clockwise vertical axis rotations during Eocene to Oligocene times (Mochales et al., 2012, Muñoz et al., 2013). A more detailed description of the geology of the area studied is provided in section 3.

2.2 Stratigraphic units

The stratigraphy of the studied area is summarized in the chronostratigraphic diagram of figure 3. Paleozoic rocks represent the base of the stratigraphic sequence, only outcropping in the Axial Zone antiformal stack to the north. Paleozoic basement was drilled at -4457 m.b.s.l. in the Huesca-1 exploration well, c. 20 km SSW of the Clamosa diapir (Fig. 4). In the Axial Zone, Paleozoic units are unconformably overlain by Permian - Lower Triassic red beds and a strongly mobile Middle-Upper Triassic layered evaporitic sequence of evaporites, shales, carbonates and minor dolorites which constitute the regional décollement of the Pyrenees. On top of this sequence, scarce bodies of Rhaetian to Lower Jurassic limestones and dolostones crop out or were drilled by exploration wells. Cretaceous rocks are represented by Cenomanian limestones and dolostones, Santonian to Campanian carbonates and Campanian to Maastrichtian limestones and calcareous sandstones. Paleocene rocks are constituted by continental mudstones and limestones (Garumn facies) that grade into marine limestones and dolostones to the northwest. Above, the lower Ilerdian (i.e., lower Ypresian) Alveolina Limestone (Mey et al., 1968) is overlain by a succession of Ilerdian marls and limestones. On top, Cuisian (i.e., upper Ypresian) carbonate platforms laterally grade into the lower part of the deep marine Aínsa slope complex deposits (Cuisian and Cuisian-Lutetian deep marine deposits, fig. 3) which were fed from the easterly fluvio-deltaic systems of the Tremp-Graus Basin (i.e., Ilerdian-Cuisian fluvio-deltaic systems). Among the latter, the Castissent Fm. (Nijman and Puigdefàbregas, 1978) represents a major fluvial progradation towards the studied area (Marzo et al., 1988).

During the Lutetian, east-sourced fluvio-deltaic systems (Fig. 3, e.g., Garrido-Megías, 1968; Nijman and Nio, 1975) in the vicinities of the Clamosa diapir were topped by the deltaic Pano Fm. (Donsellar and Nio, 1982). These fluvio-deltaic systems include a succession of fluvial mudstones, sandstones and conglomerates that grades westwards to prodelta fossiliferous

135 sandstones and mudstones and interbedded carbonate platform and reef limestones. These interbedded carbonates are found as isolated patches likely related to localized highs along the eastern and southwestern limbs of the Clamosa diapir. Eventually and especially in the western flank of the Clamosa diapir, a carbonate breccia unconformably overlies Upper Cretaceous and locally represent the base of the fluvio-deltaic sequence. Carbonate breccia is essentially made of Upper-Cretaceous sub-rounded clasts in a sandy matrix containing foraminifera and its thickness varies from few tens centimeters to few meters. On

140 top of the fluvio-deltaic deposits, the Pano Fm. is constituted by nearshore sandstones to deep-water mudstones organized in a transgressive sequence which also locally includes carbonate platforms. Fluvio-deltaic systems grade laterally into the deep marine deposits of the Aínsa slope complex (Cuisian-Lutetian deep marine deposits, fig. 3). In the vicinities of the Mediano anticline, this unit includes cm-thick beds of wackestones and packstones interbedded with non-fossiliferous marls and reef limestones topped by siliciclastic and turbiditic intervals interbedded by platform limestones units containing large

145 foraminifera. These sequences are overlain by the middle Lutetian Grustán Fm. (Garrido-Megías and Rios-Aragües, 1972) and the Entremón unit (Poblet et al., 1998) characterized by carbonate platform and reef limestones (Fig. 3). Limestones are found in the western limb of the Mediano anticline and grade basinwards into breccias.

Buil syncline — Aínsa basin — Graus-Tremp basin

Oligocene Cgs

SBZ

18a
17
16
15
14
13
12
11
10
9
8
7

Aquitan.
Chattian
Rupelian
Priabon.
Bartonian
Mid.2
Middle.1
Lutetian Middle Lower
Cuisian
Ypresian
Ilerdian
Pal
Maa
Cam San
Cen

Escanilla Fm.

Bnb

Sobrabe Fm.

Grustán-Entremón

Pano Fm.

Cuisian-Lutetian
deep marine deposits

Lutetian Carbonate
Platforms

Lower-Middle
Lutetian fluvio-
deltaic systems

Castissent Fm.

CL

Cuisian Carbonate
Platforms

Cuisian deep
marine deposits

LF

Ilerdian-Cuisian
fluvio-deltaic systems

AT

Ilerdian Marls and Limestones

Alveolina Lmst.

Garumnian

Areny Group

M
PM

Santonian-Campanian Limestones
Cenomanian Limestones

Rhaetian-Low Lias

Ofites

Upp.-Mid. Triassic

Variscan Basement

19 20 21 22 23 24 25 26 27 28 29 30 31 32 33 34 35 36 37 38 39 40 41 42 43 44 45 46 47 48 49 50 51 52 53 54 55 56 60 70 80 90 Ma

〰〰〰 Unconformity with a related sedimentary hiatus
──── Stratigraphic horizon
┈┈┈ Facies change
Thrust

7

Figure 3. Chronostratigraphic diagram showing the main stratigraphic units of the Gavarnie-Sierras and Montsec thrust sheets. Diagram is designed to cover the area around Clamosa diapir and Mediano anticline. Bnb, Buil ~~bummulitie~~nummulitic **bank;** *AT,* **Atiart unconformity;** *CL,* **Charo-Lascorz unconformity; M & PM, Montsec-Peña Montañesa thrust system; LF, La Fueba thrust system.**

155 Middle-upper Lutetian fluvial red beds of the Escanilla Fm. grade from east to west into the deltaic sandstones of the Sobrarbe Fm. (De Federico, 1981), which in turn are the lateral equivalent of the upper part of the Aínsa slope complex deposits (Cuisian-Lutetian deep marine deposits, fig. 3). The youngest marine sediments correspond to the Buil Nummulitic bank (Mateu-Vicens et al., 2012). The Escanilla Fm. expands from Bartonian to Priabonian as a fluvial formation having scarce lacustrine limestones towards the lower part of the succession. Oligocene-Miocene continental sediments unconformably lay over 160 Escanilla Fm. and older units and extensively cover the southern half of the area.

Major unconformities have been recognized along the Aínsa Oblique Zone and have been used for establishing the chronology of the different structures in the area. North of the Clamosa diapir, the most significant and well-preserved unconformities are the early-middle Cuisian L'Atiart and the latest Cuisian Charo-Lascorz truncation surfaces (Figs. 3, 4) (Soler-Sampere and 165 Garrido, 1970; Mutti et al., 1988; Muñoz et al., 1994~~; Arbués and Corregidor, 1995).~~). Flanking the Mediano anticline, an early Lutetian unconformity, namely the Mediano unconformity (Teixell and Barnolas 1995), extends along the anticline and truncates younger units to the north (e.g. Plaziat, 1984; Teixell and Barnolas, 1995) where it becomes concordant within the Lutetian deep marine deposits of the Aínsa slope complex. On top of it, Lutetian deposits exhibited a growth geometry involving some other internal unconformities that registered the kinematic evolution of the Mediano anticline (Poblet et al., 170 1998). The Mediano unconformity has been extended to the south, around the Clamosa diapir (Teixell and Barnolas, 1995) as a single surface, however locally truncated by faults. New observations and biostratigraphic information point out that the nature of the unconformities is much more complex, as it is detailed in section 3.2 and the followings.

3. The Clamosa diapir and Mediano anticline

175

3.1 Biostratigraphic data

In order to establish a time constraint regarding the development of the Clamosa diapir and its relationship with the growth of the Mediano anticline a bioestratigraphic analysis of large benthic foraminifera (LBF) was conducted. 4 paleontological sites 180 with LBF were considered (location in Fig. 5). Sampling and procedures related to the biostratigraphic analysis and systematic criteria on the classification of LBF are detailed in the appendix A.

The samples contain LBF of a well-known age distribution. Site 1 (Sample ST-1) contains Assilina maior (Heim, 1908); A. cuvillieri, (Schaub, 1981) and Nummulites campesinus (Schaub, 1966). These species are biomarkers of the Shallow Benthic Zone SBZ 12 according to Serra-Kiel et al., (1998). Site 2 (sample LP-1) contains N. manfredi (Schaub, 1966), a species corresponding also to the SBZ 12 (Serra-Kiel et al., 1998). On Site 3 (sample Cb-4) N. aff. boussaci, is found, a species representative of the SBZ 13 biozone according to Serra-Kiel et al., 1998. On Site 4 (hand sample), a Idalina berthelini (Schlumberger, 1905) was described which yields to date the rock as Lutetian.

The chronostratigraphic correlation of the SBZ 12 and SBZ 13 has been calibrated, using magnetostratographic methods, by Rodríguez – Pintó et al. (2012, 2013 and 2022). Therefore, SBZ 12 is correlated with the boundary of chron C22n - C21r and the lower part of C21n, and thus, is located in the Ypresian – Lutetian transition. According to this correlation, Sites 1 and 2 can be dated between ~49 Ma and ~47 Ma (Gradstein et al., 2020). On site 3, a SBZ 13 biomarker is found, giving a younger age. This biozone is early Lutetian and is calibrated as chron C21r to chron C20r (~47 Ma – 45.5 Ma, Gradstein et al., 2020).

SITE	SAMPLE	BIOMARKERS	SBZ biozones	Age	Age (Ma)
Site 1	ST-1	*Assilina maior, A. cuvillieri, Nummulites campesinus*	SBZ12	late Ypresian - early Lutetian	~49 - ~47
Site 2	LP-1	*N. manfredi*	SBZ12	late Ypresian - early Lutetian	~49 - ~47
Site 3	Cb-4	*N. aff. boussaci*	SBZ13	early Lutetian	~47– 45.5
Site 4	--	*Idalina Berthelini*	SBZ13-16	Lutetian	~47– ~41.4

Table 1. Biostratigraphic sites, samples, biomarkers and biozones. Sites refer to those in Figure 5.

3.2. Surface geological structure

The Clamosa diapir ~~features~~exposes a ~~triangle-shaped~~5 km-long and 2.5 km-wide outcrop of Triassic evaporites, shales and carbonates (Fig. 4). It is bounded by outcrops (ranging from 0.5 to 2km wide) of different units, consisting of the Jurassic and Upper Cretaceous to Cuisian pre-growth sequences and the Lutetian to Oligocene syn- to post-folding-diapirism sequences. To the north of the Clamosa diapir, the main structural features include the Mediano anticline, the Bruis syncline, and the Tozal de Trillo homocline (Figs. 4 and 5).

The Mediano anticline is a detachment fold cored by up to 3 km of Triassic evaporites and shales, and extends north of the Clamosa diapir for about 20 km. In the southern sector, it trends N-S, displays an east vergence, and plunges about 10º to the north (Poblet et al., 1998), before bending to a NW-SE orientation and terminating beneath the turbidites of the Aínsa basin

(Fig. 4). Northeast of the anticline, the La Fueba system consists of a SW-directed, NNW-SSE trending fold and thrust system,
210 which splays from the Montsec-Peña Montañesa thrust and mainly involves the Aínsa slope complex (Fig. 4).
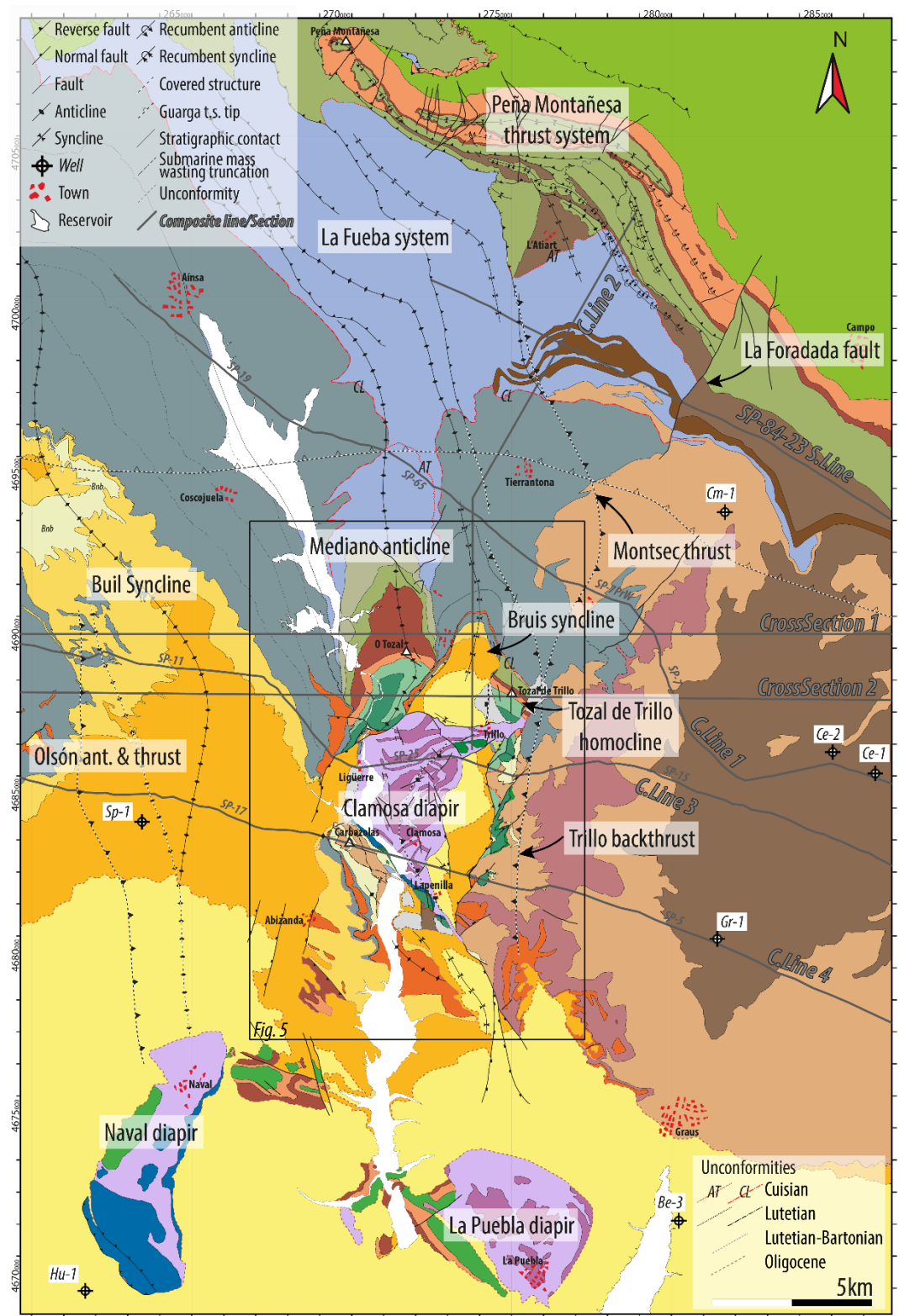
A detailed examination of the southern termination of the Mediano anticline reveals that the north plunging crest line bends towards the NNE-SSW and becomes nearly horizontal, as proved by the map trace of the Santonian-Campanian to Campanian-Maastrichtian contact (Fig. 5, 6a). Folding dates from early Lutetian to Bartonian, as evidenced by syn-folding growth strata
215 (Barnolas et al., 1991, Holl and Anastasio, 1993, Teixell and Barnolas, 1995, Bentham and Burbank, 1996, Poblet et al., 1998). In both limbs, the early Lutetian to Bartonian syn-folding sequence depicts the superposition of two single progressive unconformities (Fig. 5), defining a composite progressive unconformity with an intermediate and localized angular unconformity within the growth sequence (Poblet et al., 1998).

220 In the eastern limb of the anticline, the Palo thrust brings the steeply dipping pre- and syn-folding sequences eastwards over the Bruis syncline (Fig. 5). The Bruis syncline is a gentle fold that trends N-S, plunges to the south, and involves a succession comprising the Cuisian turbidites to the Oligocene conglomerates. Coring the syncline, the Oligocene conglomerates unconformably overlies the Bartonian-Priabonian Escanilla Fm., which in turn truncates the middle-upper Lutetian Sobrarbe Fm. along the eastern limb of the syncline. A N-S, subvertical, west dipping, normal fault bounds the Bruis syncline to the
225 east. Further east, in its footwall, a WNW-ESE trending, 70º north-dipping, Upper-Cretaceous to Ilerdian sequence (i.e., the Tozal de Trillo homocline) is unconformably overlain by upper Cuisian turbidites. Notably, the Tozal de Trillo homocline succession is attributed to the Gavarnie-Sierras thrust sheet, as its Mesozoic to Cuisian succession resembles that of the Mediano anticline.

230 The boundary between the Mediano anticline and the Clamosa diapir is marked by a diapiric, structural contact that connects to the south and west with the N010E-oriented, east-dipping Ligüerre normal fault (Fig. 5). The footwall of this fault involves Lutetian to Priabonian units unconformably overlying Upper Cretaceous carbonates and Paleocene rocks to the north, close to the Samitier Castle~~.~~ (Figs. 5, 6a). Its hanging wall includes the Lutetian to Priabonian Escanilla Fm., either overlaying or truncated by Triassic rocks of the Clamosa diapir.
235
The boundary between the Clamosa diapir and the Oligocene conglomerates of the Bruis syncline stands as a 60º north-dipping normal fault, whose lateral continuation is challenging to trace, ~~leaving open the possibility that the conglomerates also directly overlie Triassic rocks (Fig.~~ yet conglomerates dip towards the contact along most of the Oligocene outcrop pointing out that the normal fault likely continues to the east (Fig. 5). Further east, south of the Tozal de Trillo homocline, along the northeastern
240 limit of the Clamosa diapir, Triassic rocks cropping out along a W-E, 500 m wide stripe are unconformably overlain by upper Cuisian-lower Lutetian marls (as dated after foraminifera content, Site 1, Fig.5, see appendix A).

In the eastern flank of the Clamosa diapir, the fluvial sediments of the Escanilla Fm. and the Oligocene conglomerates are truncated by a system of west-dipping curved or wavy NNE-SSW normal faults (Fig. 5, 6c). Its footwall predominantly consists of Upper Cretaceous units unconformably overlain by lower to middle Lutetian deltaic and carbonate units. There, the Upper Cretaceous succession is usually capped by a meter-thick breccia of Upper Cretaceous-derived rocks that rapidly grades upwards into lower Lutetian rocks. In the hanging wall of this fault system, the Oligocene conglomerates unconformably overlie the Escanilla Fm. and the Triassic evaporites. To the southeast of the Clamosa diapir, the Lutetian succession becomes nearly horizontal and is gently truncated by the Escanilla Fm. and the Oligocene conglomerates to the south.

Legend:

- Reverse fault
- Normal fault
- Fault
- Anticline
- Syncline
- Well
- Town
- Reservoir
- Recumbent anticline
- Recumbent syncline
- Covered structure
- Guarga t.s. tip
- Stratigraphic contact
- Submarine mass wasting truncation
- Unconformity
- Composite line/Section

Labels on map:

- Peña Montañesa thrust system
- La Fueba system
- La Foradada fault
- Ainsa
- L'Atiart
- AT
- Campo
- SP-84-23 S.Line
- Montsec thrust
- Cm-1
- CrossSection 1
- CrossSection 2
- Mediano anticline
- Buil Syncline
- Bruis syncline
- Coscojuela
- Tierrantona
- O Tozal
- Tozal de Trillo
- Tozal de Trillo homocline
- Trillo
- Olsón ant. & thrust
- Ligüerre
- Clamosa diapir
- Carbazolas
- Clamosa
- Trillo backthrust
- Lapenilla
- Ce-2
- Ce-1
- C.Line 1
- C.Line 3
- Sp-1
- Gr-1
- C.Line 4
- Abizanda
- Fig. 5
- Naval
- Naval diapir
- La Puebla diapir
- Graus
- Be-3
- La Puebla
- Hu-1

Unconformities:

- AT   CL   Cuisian
- Lutetian
- Lutetian-Bartonian
- Oligocene

5km

250

Figure 4. Geological map of the area studied. See figure 3 for the colour legend of stratigraphic units. Main structural features described in the text are labelled. Dark grey lines represent seismic sections, composite lines and cross-sections traces. Note that black-white dashed lines denote buried structural features. The tip line of the Guarga basement thrust sheet is represented as a dashed black and white line with open black arrows. Southern and northern areas are adapted from ~~Barnolas~~Teixell et al. (1994a, b~~;~~) Robador-Moreno and Zamorano-Cáceres (1999) and Santolaria et al. (2014).
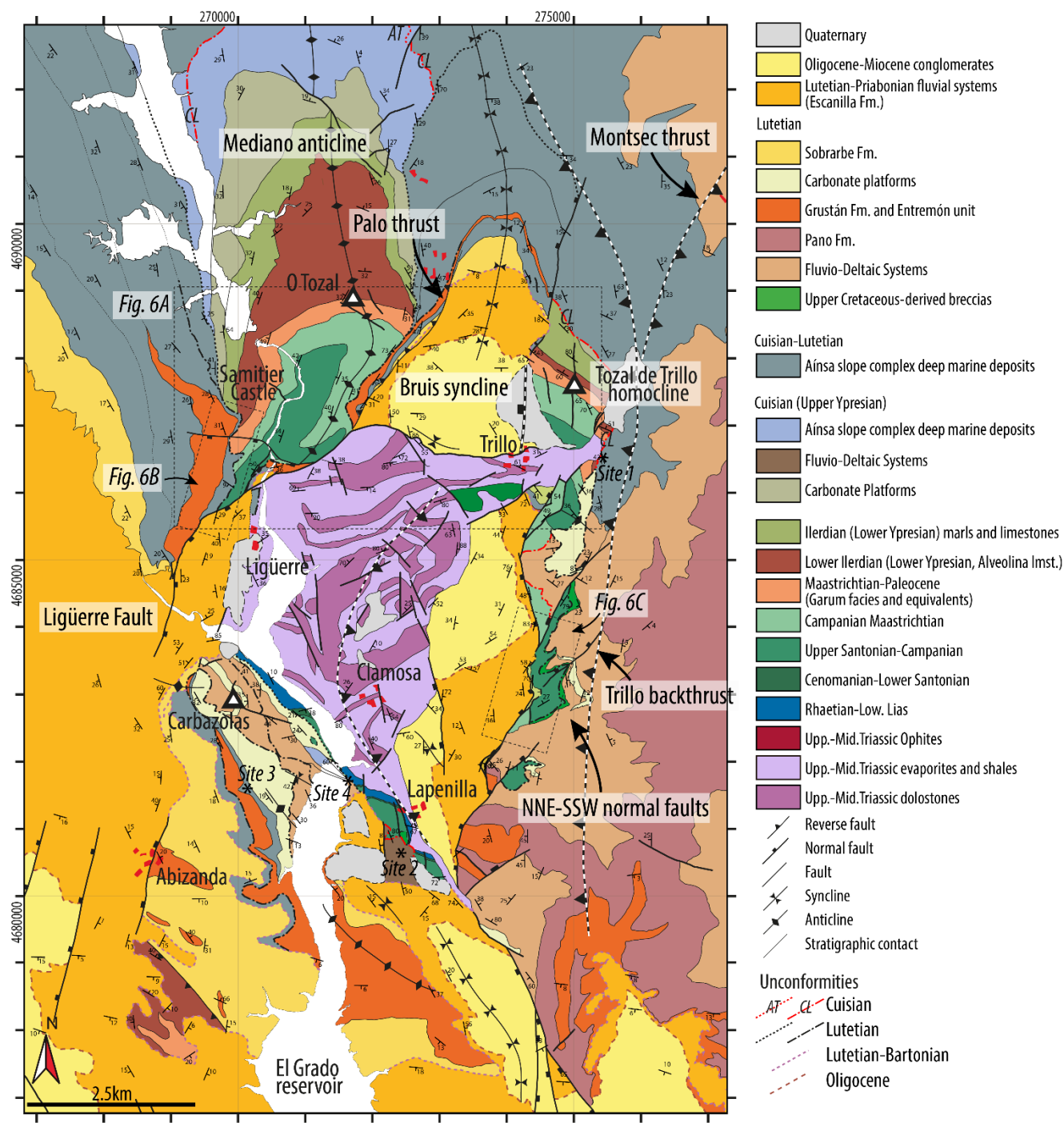
Legend:

- Quaternary
- Oligocene-Miocene conglomerates
- Lutetian-Priabonian fluvial systems (Escanilla Fm.)

Lutetian
- Sobrarbe Fm.
- Carbonate platforms
- Grustán Fm. and Entremón unit
- Pano Fm.
- Fluvio-Deltaic Systems
- Upper Cretaceous-derived breccias

Cuisian-Lutetian
- Aínsa slope complex deep marine deposits

Cuisian (Upper Ypresian)
- Aínsa slope complex deep marine deposits
- Fluvio-Deltaic Systems
- Carbonate Platforms

- Ilerdian (Lower Ypresian) marls and limestones
- Lower Ilerdian (Lower Ypresian, Alveolina lmst.)
- Maastrichtian-Paleocene (Garum facies and equivalents)
- Campanian Maastrichtian
- Upper Santonian-Campanian
- Cenomanian-Lower Santonian
- Rhaetian-Low. Lias
- Upp.-Mid.Triassic Ophites
- Upp.-Mid.Triassic evaporites and shales
- Upp.-Mid.Triassic dolostones

- Reverse fault
- Normal fault
- Fault
- Syncline
- Anticline
- Stratigraphic contact

Unconformities
- AT CL Cuisian
- Lutetian
- Lutetian-Bartonian
- Oligocene

Map labels: Mediano anticline, Montsec thrust, Palo thrust, O Tozal, Fig. 6A, Samitier Castle, Bruis syncline, Tozal de Trillo homocline, Fig. 6B, Trillo, Site 1, Ligüerre, Ligüerre Fault, Fig. 6C, Clamosa, Carbazolas, Trillo backthrust, Site 3, Site 4, Lapenilla, NNE-SSW normal faults, Abizanda, Site 2, El Grado reservoir, 2.5km

14

Figure 5. Geological map of the Mediano anticline-Clamosa diapir area showing the structural features described in the text and paleontological sites included in the biostratigraphic analysis shown in the appendix A. Partly adapted from ~~Barnolas~~Teixell et al. (1994b).
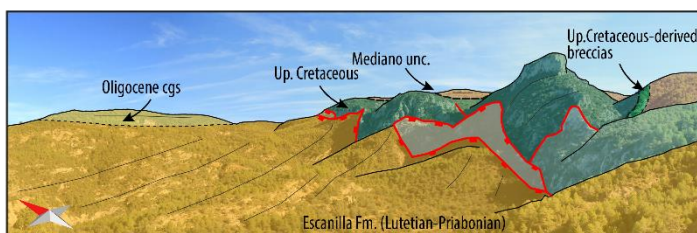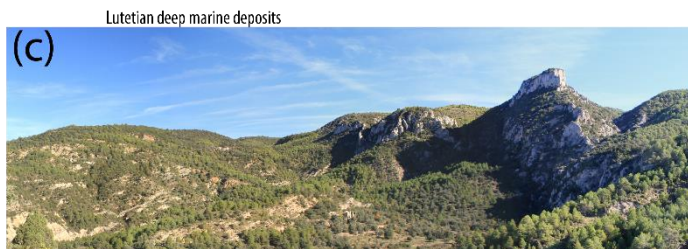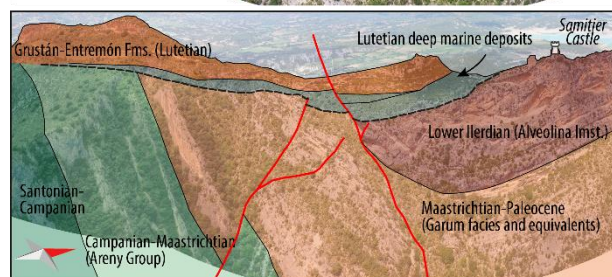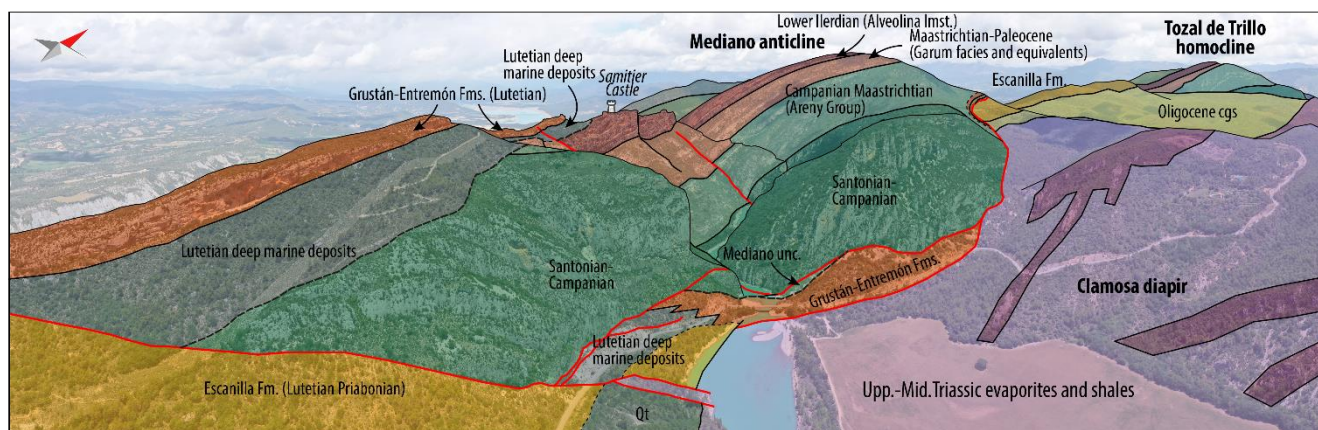
260

(a)

Lower Ilerdian (Alveolina lmst.)
Mediano anticline
Maastrichtian-Paleocene
(Garum facies and equivalents)
Tozal de Trillo homocline

Lutetian deep marine deposits
Grustán-Entremón Fms. (Lutetian)
Samitjer Castle
Campanian Maastrichtian (Areny Group)
Escanilla Fm.
Oligocene cgs

Lutetian deep marine deposits
Santonian-Campanian
Santonian-Campanian
Mediano unc.
Grustán-Entremón Fms.
Clamosa diapir

Escanilla Fm. (Lutetian Priabonian)
Lutetian deep marine deposits
Qt
Upp.-Mid. Triassic evaporites and shales

(b)

Lutetian deep marine deposits

(c)

Grustán-Entremón Fms. (Lutetian)
Lutetian deep marine deposits
Samitjer Castle

Lower Ilerdian (Alveolina lmst.)

Santonian-Campanian
Maastrichtian-Paleocene (Garum facies and equivalents)

Campanian-Maastrichtian (Areny Group)

Oligocene cgs
Up. Cretaceous
Mediano unc.
Up. Cretaceous-derived breccias

Escanilla Fm. (Lutetian-Priabonian)

Figure 6. (a), Drone image of the northern boundary of the Clamosa diapir and the Mediano anticline and its interpretation. (b), Close up view of northwestern flank of the Clamosa diapir and Mediano anticline. (c), Interpreted picture of the NNE-SSW trending, west-dipping extensional faults related to the collapse of the diapir during Oligocene. See their location in Fig. 5.

265

In the southwestern flank of the Clamosa diapir, there is a 5.5 km long, NW-SE oriented, outcrop of folded and faulted Jurassic dolostones and Upper Cretaceous limestones and sandstones (Fig. 5). In the Carbazolas sector, the Mesozoic sequence is overlain by Lutetian carbonates, followed by Lutetian fluvio-deltaic units, carbonates and turbidites, generally trending NW-SE. This sequence features several internal unconformities, which may resemble or be equivalent to those found along the

270 limbs of the Mediano anticline. This sequence is also unconformably overlain by the middle-upper Lutetian Sobrarbe Fm. and by the Lutetian-Priabonian Escanilla Fm. To the southeast, near Lapenilla village, Triassic evaporites extend for 2.5 km along a narrow band, trending NW-SE. There, upper Cuisian to lower Lutetian fluvio-deltaic rocks (as dated after foraminifera content, Site 2, Fig.5, see appendix A), unconformably overlie the Triassic to Upper Cretaceous succession. This stripe of Triassic evaporites links to a set of NNW-SSE to N-S faults that die out into the Oligocene conglomerates to the south (Fig.

275 5). To the west of the Mediano anticline and the Clamosa diapir, the most prominent structure at surface is the gently south-plunging Buil syncline (Fig. 4). The southern part of the area is extensively covered by Oligocene conglomerates, except for localized outcrops of folded and faulted Upper Cretaceous to Ilerdian rocks and Triassic evaporites coring elongated to rounded diapirs (Naval and La Puebla respectively) (Figs. 2, 4).

280 **3.3. Seismic interpretation and subsurface structure**

To illustrate the subsurface structure of the studied area, 12 seismic lines and 2 key cross-sections are used (see Fig. 4 for location and Figs. 7 and 8 for their interpretation). These seismic lines and cross-sections are strategically located: to the north, along the Aínsa basin (SP-84-23); across the Mediano anticline and the Montsec thrust sheet front (Composite Line 1, including

285 the seismic profiles SP-19, SP-65, SP-7PrW and SP-7 and Cross Sections 1 and 2; see Fig. 7); across the La Fueba system and along the Bruis syncline (Composite Line 2, including seismic profile SP-84-19); and across the Clamosa diapir (Composite Lines 3 and 4 including the seismic profiles SP11, SP25, SP15, SP-17 and SP-5; see Fig. 8). The traces of deep-seated and buried structures derived from seismic interpretations and the construction cross-sections are represented in Fig. 4 as black and white dashed lines, aiding the description of the subsurface structure. The uninterpreted version of these seismic lines is

290 provided in the Appendix B.

3.3.1. The Montsec-Peña Montañesa thrust sheet

In the north of the study area, the Peña Montaseña thrust system links with the L'Atiart thrust, to the south and continues at

295 depth with the Montsec thrust (SP-84-23 line, Figs. 4 and 7). The Montsec thrust sheet involves a Jurassic-Upper Cretaceous

17

to Ilerdian succession, slightly truncated by the La Foradada tear fault and, further west, the thrust branches off into several thrusts belonging to the La Fueba System. Along Composite Line 1, the Montsec thrust sheet shows a similar geometry as in SP-84-23, but the La Fueba system and La Foradada fault are absent as they do not extend that far south (Fig. 4). To the south, the Montsec thrust acquires a NNE-SSW orientation and is truncated at depth by the Trillo backthrust (see Fig. 4 and Cross

300 Sections 1 and 2 and Composite Lines 3 and 4, Figs. 7 and 8). The cross-sections generally show the Montsec-Peña Montañesa thrust sheet as a gently folded Triassic to Ilerdian succession, with nearly parallel seismic reflectors that thin towards the west and south (e.g. Soto et al., 2002; Fernández et al., 2012). In contrast, Cuisian – Lutetian sediments show tens of kilometres wide growth strata geometries, generally thickening towards the west (see Composite line 1; (Fig. 7). The truncation of the Montsec thrust sheet by the Trillo backthrust suggests that the frontal tip of the Montsec thrust was truncated, uplifted, exhumed

305 and eroded (see below and section 5 for further discussions).

3.3.2 The Gavarnie-Sierras thrust sheet

The Gavarnie-Sierras thrust sheet in the footwall of the Montsec-Peña Montañesa thrust sheet features a laterally variable

310 geometry. Conversely to the Montsec-Peña Montañesa, the Gavarnie-Sierras thrust sheet shows a shorter structural wavelength, localized growth strata geometries hundreds-of-meters-wide, and a markedly thinner Triassic to Ilerdian succession that maintains the western and southern thinning trends.

To the north of the study area, in the footwall of the Montsec thrust, the Gavarnie-Sierras thrust sheet is distinctly imaged as a

315 nearly parallel sequence detached over the Guarga basement thrust sheet, which in turn thrust over the Ebro basin foreland units (SP-84-23 and Composite Line 1, Fig. 7). In map view, the Guarga thrust has a curved shape with an overall N100W orientation, i.e. highly oblique to cover structures (Fig. 4). Along Composite Line 1 (Fig. 7) the Mediano anticline is imaged as an asymmetric, east-verging, open anticline, with its eastern limb truncated by a thrust.

320 To the south, the Mediano Anticline tightens and increases in amplitude. In cross-section 1 (Fig. 7), it features a wavelength of about 8 km and an amplitude of 3.6 km. The anticline appears as a slightly asymmetric detachment fold cored by a large accumulation of Triassic evaporites, with its western and eastern limbs dipping 40 to 70-80 degrees to the west and east, respectively. Its western flank abuts the South Pyrenean sole thrust, but its eastern flank does not; it occupies a higher structural position below the Bruis syncline (Fig. 7, cross-section 1). Further south, along cross-section 2, the eastern flank of the

325 Mediano anticline reduces to a thousand-meter-wide panel of Upper Cretaceous, with the Bruis syncline directly overlying Triassic evaporites. Composite Line 2 (Fig. 8) better illustrates the north to south shallowing of the Mediano anticline eastern limb, note this composite line run nearly parallel to it (Fig. 4). In the northern part of this composite line, the Montsec thrust and the La Fueba system thrust over a seismically well-imaged Upper Cretaceous-Lower Eocene sequence of the Gavarnie-Sierras thrust sheet. Both the Montsec-Peña Montañesa and Gavarnie-Sierras thrust sheets are tilted by the Guarga basement

thrust sheet, with the tip point located halfway along the section. Seismic interpretation reveals that there is little to no Triassic evaporites between the Gavarnie-Sierras and the Guarga basement. Yet, they are decoupled. South of the tip point, the Gavarnie-Sierras sequence progressively acquires a north-dipping inclination as it approaches the Clamosa diapir (Fig. 8). Unconformably atop the Gavarnie-Sierras sequence, the Lutetian slope deposits of the Bruis syncline gently dip southward, towards the Clamosa diapir. And, unconformably on top of them, the Escanilla Fm. and the Oligocene conglomerates define a restricted trough towards the Clamosa diapir (Fig. 8, note that this section runs ~~parallel~~subparallel to the axis of the Bruis syncline).

Back to the W-E cross-sections (Fig. 7), a west dipping normal fault separates the Lutetian to Oligocene rocks of the Bruis syncline from the Tozal de Salinas homocline, which thrust over the Peña Montañesa-Montsec thrust sheet succession (see Trillo backthrust in Fig. 7, cross-sections 1 and 2). ~~A triangular piece of the Gavarnie-Sierras units remains in the footwall of the Montsec thrust and the Trillo backthrust.~~

Along the Clamosa diapir transects, in the western limb of the Mediano anticline, the pre-folding succession dips approximately 40-50 degrees to the west, while near the Clamosa diapir, it becomes nearly vertical (SP-25, Composite line 3, Fig. 8) or is folded and overturned (Composite line 4, Fig. 8). Along the western flank of the diapir, Lutetian growth strata lie moderately to gently dipping in SP-11 (Composite line 3, Fig. 8) but are folded and faulted in Composite Line 4 (Fig. 8). The top of the Clamosa diapir is bounded by a set of diapir-converging faults that involve limited Upper Cretaceous rocks but mostly Lutetian to Oligocene units, which are suggested to lie directly on top of Triassic evaporites (Fig. 8). The eastern boundary of the diapir is represented by the Trillo backthrust that brings the Upper Cretaceous units to the surface (Fig. 5 and Fig. 8) and truncates the Montsec thrust (as in previous sections). The Trillo backthrust is a crucial structure that explains the absence of the trace of the Montsec thrust at surface east of the Clamosa diapir, a puzzling area that has challenged the connection between the Montsec thrust and the Peña Montañesa thrust (Fig. 4). Yet, the interpretation of the Trillo backthrust can be regarded as debatable: its trace does not crop out and it is not properly imaged in seismic lines. However, our backthrust interpretation is based on: i) the fact that Upper Cretaceous-Ilerdian sequence with Gavarnie-Sierras Marginales affinity (Salinas de Trillo homocline and eastern flank of the Clamosa diapir) stands in a higher structural position with respect to its time-equivalent sequence in the Montsec thrust sheet (which is approximately two-times thicker) (Composite Lines 3 and 4, Fig. 8), ii) the apparent absence of the tip of the Montsec thrust sheet as observed further north (e.g. Composite Line 1, Fig.7) and iii) the presence of a triangular piece interpreted as a remnant of the Gavarnie-Sierras units in the footwall of both the Montsec thrust and the Trillo backthrust. Interpretation supported by the presence of subhorizontal reflectors in the western termination of the SP-15 and SP-25 lines (Composite Line 3, fig. 8 and Appendix B, Fig.Bd). Calculated slip is maximum in the vicinities of the Clamosa diapir (c. 5km, Composite Lines 3 and 4, Fig. 8) and decreases to the north (c.1.5km in Cross-section 1, Fig. 7).
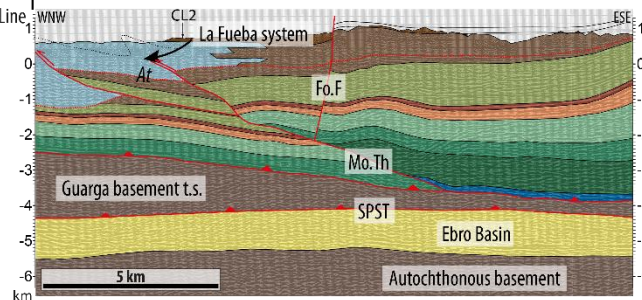
To the west of the Clamosa diapir and Mediano anticline, the Buil syncline appears as an open syncline. Beneath it, subsurface data reveal the existence of the Olsón anticline, a thrust-related anticline fossilized by Lutetian deposits. In map view, the Olsón anticline trends N-S to N150E for approximately 11 km (Fig. 4) and links with the Naval diapir.

Gavarnie-Sierras thrust sheet | Montsec-Peña Montañesa thrust sheet

Mo.Th, Montsec thrust
Tr.BTh, Montsec backthrust
SPST, South Pyrenean Sole Thrust
Fo.F, La Foradada Fault
Pa.Th, Palo thrust
Med.Ant, Mediano anticline
Br.Syn, Bruis syncline
Ols.Th&Ant, Olsón thrust and anticline

Unconformities
At — CL — Cuisian
Lutetian
Lutetian-Bartonian
Oligocene

SP-84-23 Seismic Line — WNW — CL2 — ESE
La Fueba system
At
Fo.F
Mo.Th
Guarga basement t.s.
SPST
Ebro Basin
Autochthonous basement
5 km

Gavarnie-Sierras thrust sheet | Montsec-Peña Montañesa thrust sheet

Composite Line 1 — WNW — CL2 — CS1 — CS2 — ESE
CL
Med.Ant
At
Med.Th
Mo.Th
Guarga basement t.s.
SPST
Ebro Basin
Autochthonous basement
5 km
Seismic lines   SP-19   SP-65   SP-7PrW   SP-7

Gavarnie-Sierras thrust sheet | Montsec-Peña Montañesa thrust sheet

Cross-Section 1 — W — Med.Ant — CL2 — CL1 — E
CL
Br.Syn
At
Ols.Th&Ant
Tr.BTh
Mo.Th
SPST
Ebro Basin
Autochthonous basement
5 km

Gavarnie-Sierras thrust sheet | Montsec-Peña Montañesa thrust sheet

Cross-Section 2 — W — CL3 — Med.Ant — CL2 — CL1 — E
Br.Syn
CL
Ols.Th&Ant
Tr.BTh
Mo.Th
SPST
Ebro Basin
Autochthonous basement
5 km

Oligocene-Miocene conglomerates

Lutetian-Priabonian fluvial systems (Escanilla Fm.)

Lutetian
Sobrarbe Fm.
Grustán Fm.-Entremón unit Pano Fm.
Fluvio-Deltaic Systems
Carbonate platforms

Cuisian-Lutetian
Aínsa slope complex deep marine deposits
Cuisian (Upper Ypresian)
Aínsa slope complex deep marine deposits
Castissent Fm.
Fluvio-Deltaic Systems
Carbonate Platforms

Ilerdian marls and limestones
Lower Ilerdian (Alveolina lmst.)
Maastrichtian-Paleocene (Garum facies and equivalents)
Campanian Maastrichtian
Upper Santonian-Campanian

Cenomanian-Lower Santonian
Rhaetian-Low. Lias
Upp.-Mid.Triassic evaporites and shales
Upp.-Mid.Triassic dolostones
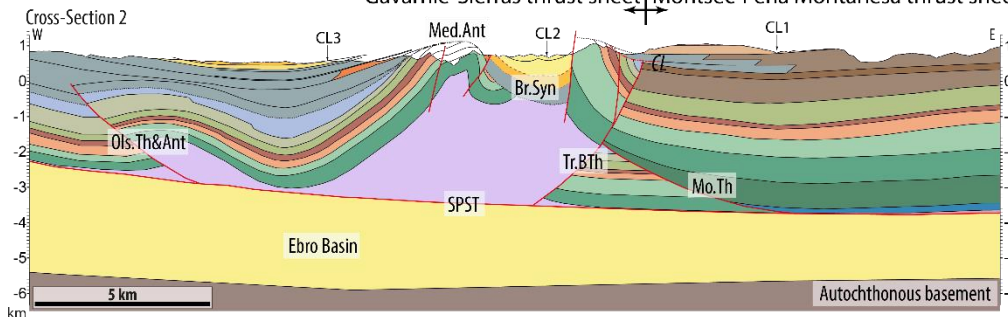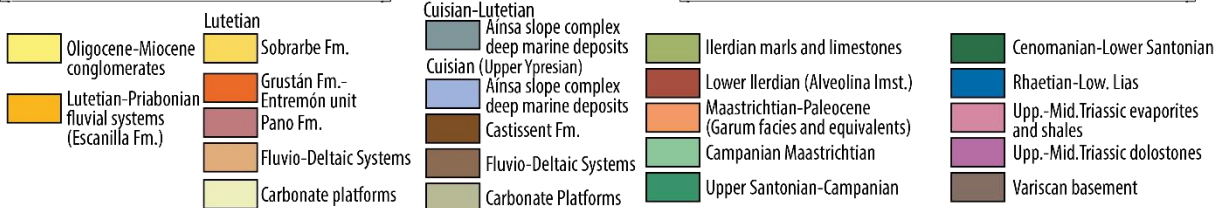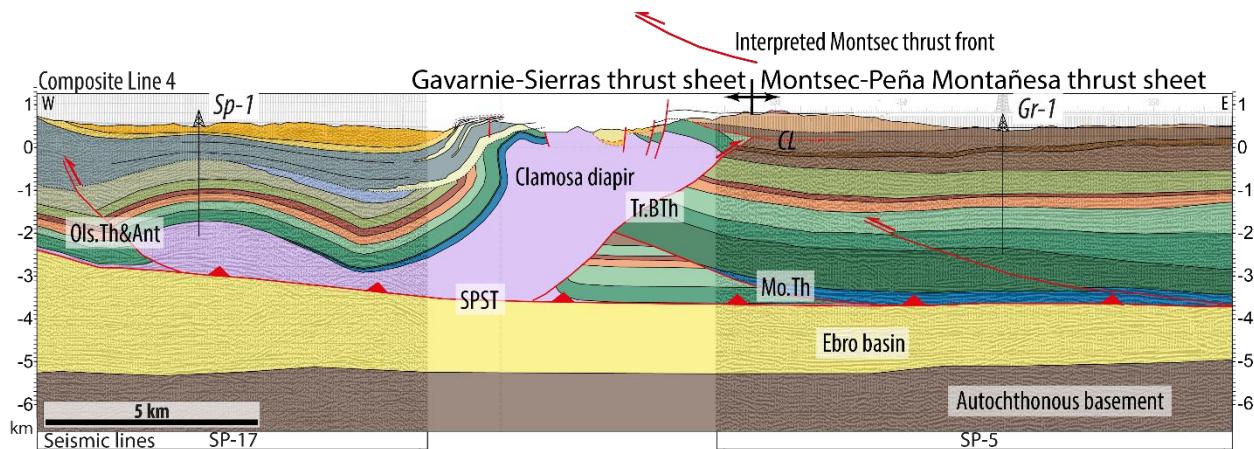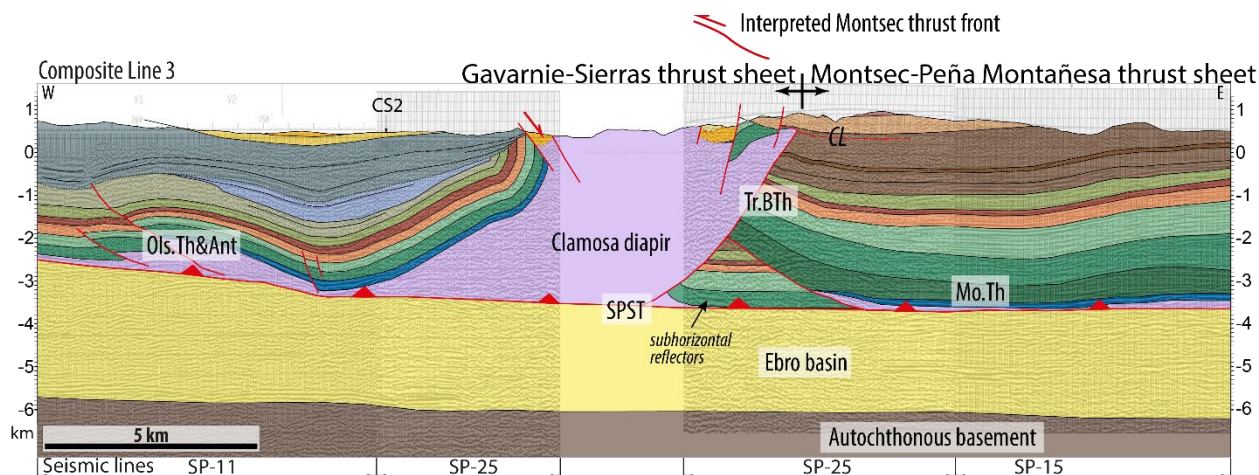Variscan basement

21

Figure 7. Cross sections and interpreted seismic lines illustrating the subsurface structure of the Montsec-La Fueba system (SP-84-23 seismic line), and the north to south along strike variability of the Montsec-Mediano anticline structures (Composite line 1, Cross-section 1 and Cross section 2). See fig. ~~4 for location.~~4 for location and appendix B for the uninterpreted version of the seismic lines. Note that the thickness of the Upper Cretaceous to Ilerdian sequence in the Tozal de Trillo Homocline (Cross-sections 1 and 2) and the growth of the same sequence in cross-section 2 are apparent due to the low angle between the section traces and the strike of these tilted sequences there.

Mo.Th, Montsec thrust
Tr.BTh, Montsec backthrust
SPST, South Pyrenean Sole Thrust
Fo.F, La Foradada Fault
Pa.Th, Palo thrust
Med.Ant, Mediano anticline
Br.Syn, Bruis syncline
Ols.Th&Ant, Olsón thrust and anticline
Unconformities
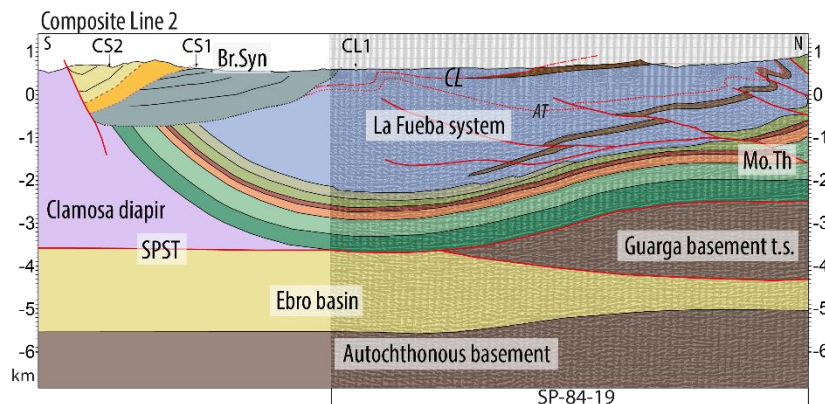— Cuisian
— Lutetian
— Lutetian-Bartonian
— Oligocene

Legend:
Oligocene-Miocene conglomerates
Lutetian-Priabonian fluvial systems (Escanilla Fm.)

Lutetian
Sobrarbe Fm.
Grustán Fm.-Entremón unit Pano Fm.
Fluvio-Deltaic Systems
Carbonate platforms

Cuisian-Lutetian
Aínsa slope complex deep marine deposits
Cuisian (Upper Ypresian)
Aínsa slope complex deep marine deposits
Castissent Fm.
Fluvio-Deltaic Systems
Carbonate Platforms

Ilerdian marls and limestones
Lower Ilerdian (Alveolina lmst.)
Maastrichtian-Paleocene (Garum facies and equivalents)
Campanian Maastrichtian
Upper Santonian-Campanian

Cenomanian-Lower Santonian
Rhaetian-Low. Lias
Upp.-Mid.Triassic evaporites and shales
Upp.-Mid.Triassic dolostones
Variscan basement

375

23

Figure 8. Interpreted Composite lines 2, 3 and 3 illustrate the subsurface structure of the Montsec-Clamosa diapir system. See fig. 4 for location. and appendix B for the uninterpreted version of the seismic lines. Sp-1: Surpirenaica-1 exploration well. Gr-1: Graus-1 exploration well.

380   **4. Structural evolution of the Clamosa diapir and Mediano anticline in the western South Pyrenean Central Salient**

This section aims to frame the formation of the Clamosa diapir and the Mediano anticline within the structural and kinematic evolution of the western half of the South Pyrenean Central Salient, and contextualize the formation and evolution of salt diapirs in contractional settings. As introduced earlier, this area of the Pyrenees is characterized by along strike structural

385   changes and N-S trending structures that underwent up to 80º of syn-orogenic vertical axis clockwise rotation (Mochales et al., 2012; Muñoz et al., 2013). In this context, we propose that the Clamosa diapir is a purely contractional diapir whose salt accumulation is inherited from a Triassic extensional basin that was incorporated into the fold-and-thrust belt system together with the formation of the Trillo backthrust and the Mediano anticline. So, we interpret the formation of the Clamosa diapir as a combination of salt inflation, folding and thrusting, followed by piercing of the cover triggered by erosion and longitudinal

390   stretching upon vertical axis rotation. Finally, the diapir underwent extensional collapse. In the following, we provide a detailed and justified evolutionary model for the Clamosa diapir, the Mediano anticline and La Fueba thrust system. The proposed evolution is illustrated and discussed through schematic sections (Fig. 9) and a plan view restoration (Fig. 10).

The Clamosa diapir belongs to a salt tectonics province in the Gavarnie-Sierras thrust sheet, characterized by thick Middle-

395   Upper Triassic evaporites, mudstones and carbonates. In this province, diapirs have pierced the Upper Cretaceous to Miocene succession and have been fed from a thick salt layer as revealed by geological surface and subsurface data, and gravity data (Fig. 4, Santolaria et al., 2016, 2024). A key point in the study area is the original distribution and thickness of the Triassic evaporites and the timing of interpreted salt inflation events. Burrel and Teixell (2021) postulated a thick and continuous Triassic evaporitic basin, over a faulted basement, thickening northwards from 1km in the southern Gavarnie-Sierras thrust

400   sheet to 3km beneath the Montsec thrust sheet. These authors suggest that accommodation space of Jurassic to Upper Cretaceous basins resulted from downbuilding and the surrounding salt walls fed by salt flow in multiple directions (Burrel and Teixell, 2021). They suggested that downbuilding coexisted with shortening since Palaeocene, and the salts~~salt~~ walls were subsequently squeezed during the Paleogene. On the other hand, Santolaria et al. (2016) suggested that the salt in the Gavarnie-Sierras thrust sheet was inflated by salt flow evacuated from beneath the Montsec thrust sheet as it was transported to the

405   south. Conversely, Hudec et al. (2021) proposed that the salt province of the Gavarnie-Sierras thrust sheet developed in an isolated southern Triassic graben and that salt flowed northward from Jurassic to Upper Cretaceous times. Salt would have been inflated against the structural high bounding the basin northwards that would coincide with the Montsec thrust sheet and the Graus-Tremp piggy-back basin. The Montsec thrust would correspond to a salt wall developed since late Jurassic, with its western tip corresponding top the Clamosa diapir (Hudec et al., 2021). To tackle the question of the pre-shortening distribution

24

of Triassic evaporites, we focused on the distribution of some distinct Mesozoic units around the Clamosa diapir, mainly the ~~lower Jurassic carbonates and the postrift upper Cenomanian limestones (Fig. 3).~~Lower Jurassic carbonates and the postrift Upper Cenomanian limestones (Fig. 3). In the study area, along the Gavarnie-Sierras Marginales thrust sheet, Middle-Upper Triassic evaporites are usually topped by Upper Cretaceous rocks, therefore, the presence of Lower Jurassic carbonates or Upper Cenomanian limestones represents an anomaly. Hettangian carbonates are also observed around the diapirs of the salt tectonics domain extending south of the Clamosa diapir (as in the Naval diapir, Fig. 1, Santolaria et al., 2014) and are also unevenly distributed along some of the southern thrust sheets of the central Sierras Marginales (e.g. Burrel and Teixell, 2021). We propose that presence of these rocks relates to their deposition over relatively thicker Middle-Upper Triassic depocenters: such depocenter were prone to accommodate the Lower Jurassic carbonates and later on the Upper Cenomanian limestones, that might sink by differential loading, and prevent their erosion. The Triassic evaporites were deposited during the last stages of the first rifting event that affected Iberia during the break-up of Pangea (López-Gómez et al., 2019). Above, the Hettangian carbonates represent either the last stages of rifting or the start of the sag phase. Triassic basins have been completely inverted and deformed during Pyrenean deformation, yet some of them can be reconstructed (López-Gómez et al., 2019). In the Clamosa diapir, the presence of the ~~lower~~Lower Jurassic carbonates at its southern margin suggests the existence of an ~~upper~~Upper Triassic depocenter, in contraposition of the northern margin of the diapir where the Upper Cretaceous sediments rest directly above the Keuper, pointing out to the existence of a structural high (Fig. 9a, b). Interestingly, a 20-30 meters-thick Upper Cenomanian sequence is also preserved in what it was the southern basin, and which is nowadays the southwestern limb of the Clamosa diapir (Fig. 5). This sequence developed northwards in the Montsec thrust sheet above the Middle-Upper Triassic evaporites and a thicker and more complete Jurassic succession, on what it was the proximal domain of the North Iberian Early Cretaceous rifted margin. ~~Hettangian carbonates are also observed around the diapirs of the salt tectonics domain extending south of the Clamosa diapir.~~Thus, in the central part of the study area a southern salt basin would be separated from a northern basin by a structural high, aligning with the interpretation by Hudec et al. (2021). However, from our observations, this high is located south of the Montsec thrust and would have controlled the location of the Montsec thrust as well as the Trillo backthrust. Moreover, the southern basin, would be oblique to the northern one and terminates to the west. It would be most probably connected with the northern salt basin eastward, as suggested by the deposition of the ~~upper~~Upper Cenomanian limestones. In any case, the observed salt structures, as well as thrusts and related folds would have been controlled by the pre-shortening 3d configuration of the Triassic basins and highs.

The absence of any ~~middle~~Middle Jurassic to Upper Cretaceous stratigraphic record in the western Sierras Marginales, including the salt province above referred, do not support the idea of salt flow during this time, and consequently the formation of salt structures~~, as suggested by Hudec et al., 2021 and Burrel and Teixell, (2021).~~. The Santonian to Paleocene succession formed a south and west-thinning sedimentary wedge above the southern Triassic basin, as well as atop of the structural high and the Peña Montañesa-Montsec thrust sheet (Fig. 9b). There is no evidence of local thickness changes of this succession, discarding any local salt movement in this area during Late Cretaceous to late Cuisian (Fig. 9b), contrary to what is observed

eastward in the Gavarnie-Sierras thrust sheet (Hudec et al., 2021; Burrel and Teixell, 2021; Ramirez-Perez et al., 2024).

445 Deposition of this Upper Cretaceous to Paleocene succession occurs at the same time as the Cotiella-Bóixols thrust sheet and related basement thrust sheets were already emplaced north of the studied area (Fig. 10b).

Later, between Paleocene and Cuisian, the Montsec thrust emplaced as a SSW-directed thrust (Fig. 10c) coevally to the sedimentation of fluvio-deltaic and deep marine sequences along the Tremp-Graus and Aínsa basin slope complex,

450 respectively. The Montsec thrust likely nucleated at the southern pinch-out of the northern salt basin (note that pinch-out does not necessarily refer to the disappearance of Triassic evaporites but to a significant thinning of them that may represent a mechanical discontinuity in the salt décollement) (Fig. 9c).
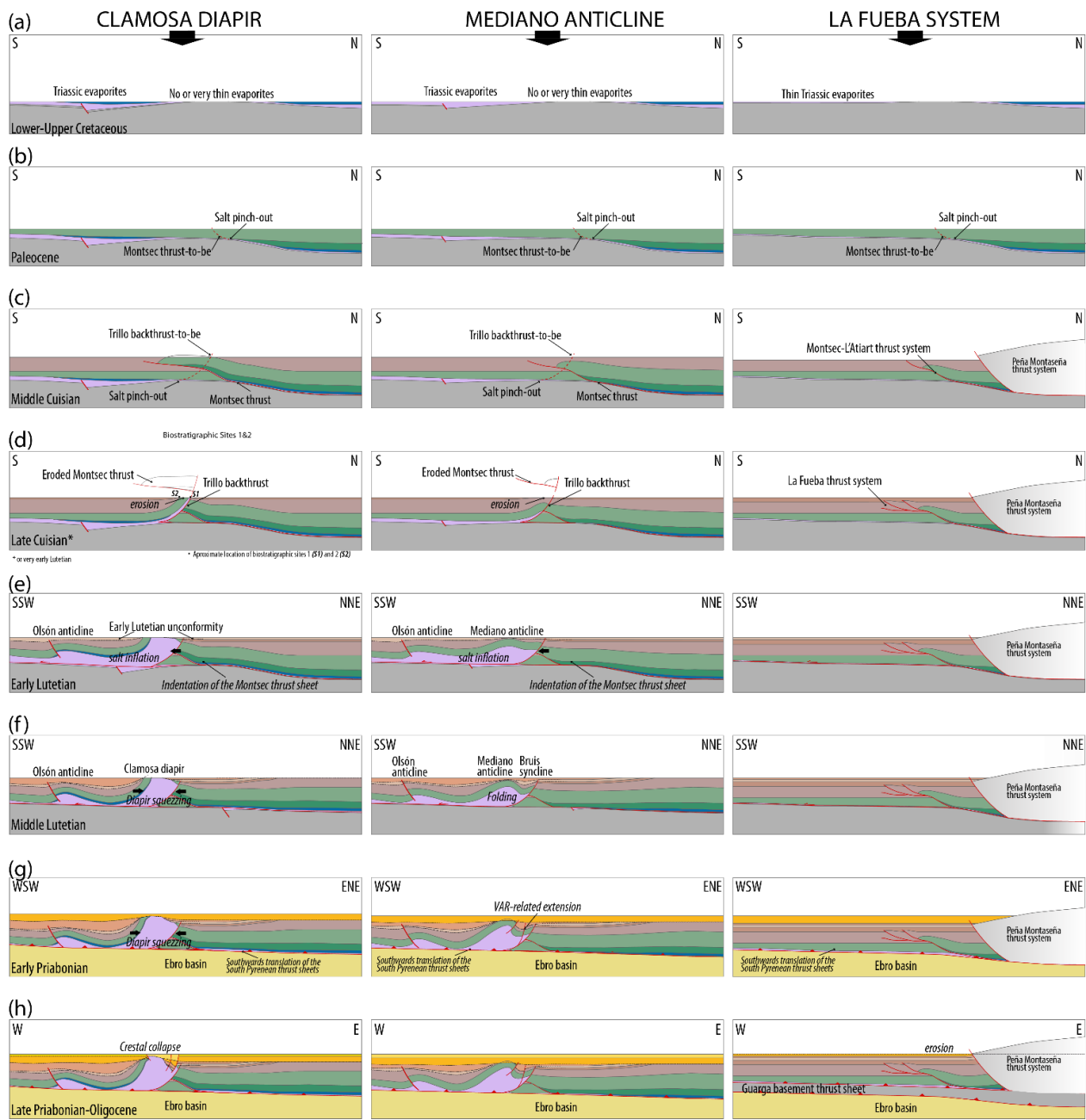
Figure 9. Stepped reconstruction that illustrates the along strike differences of the formation of Clamosa diapir (left column), the Mediano anticline (central column) and the Peña Montañesa-La Fueba system (right column). Sketches gather representative surface and subsurface geological information; they are not structural restorations. Obliqueness, out-of-plane deformation and vertical axis rotation prevent any reliable cross-section restoration. Yet, some of the ideas illustrated here come from local and punctual restorations. Note the change in the orientation of the sketches. Such changes account for the Middle to Late Eocene vertical axis rotation. An approximate location of the section is shown in the plan view reconstruction of Fig. 10.
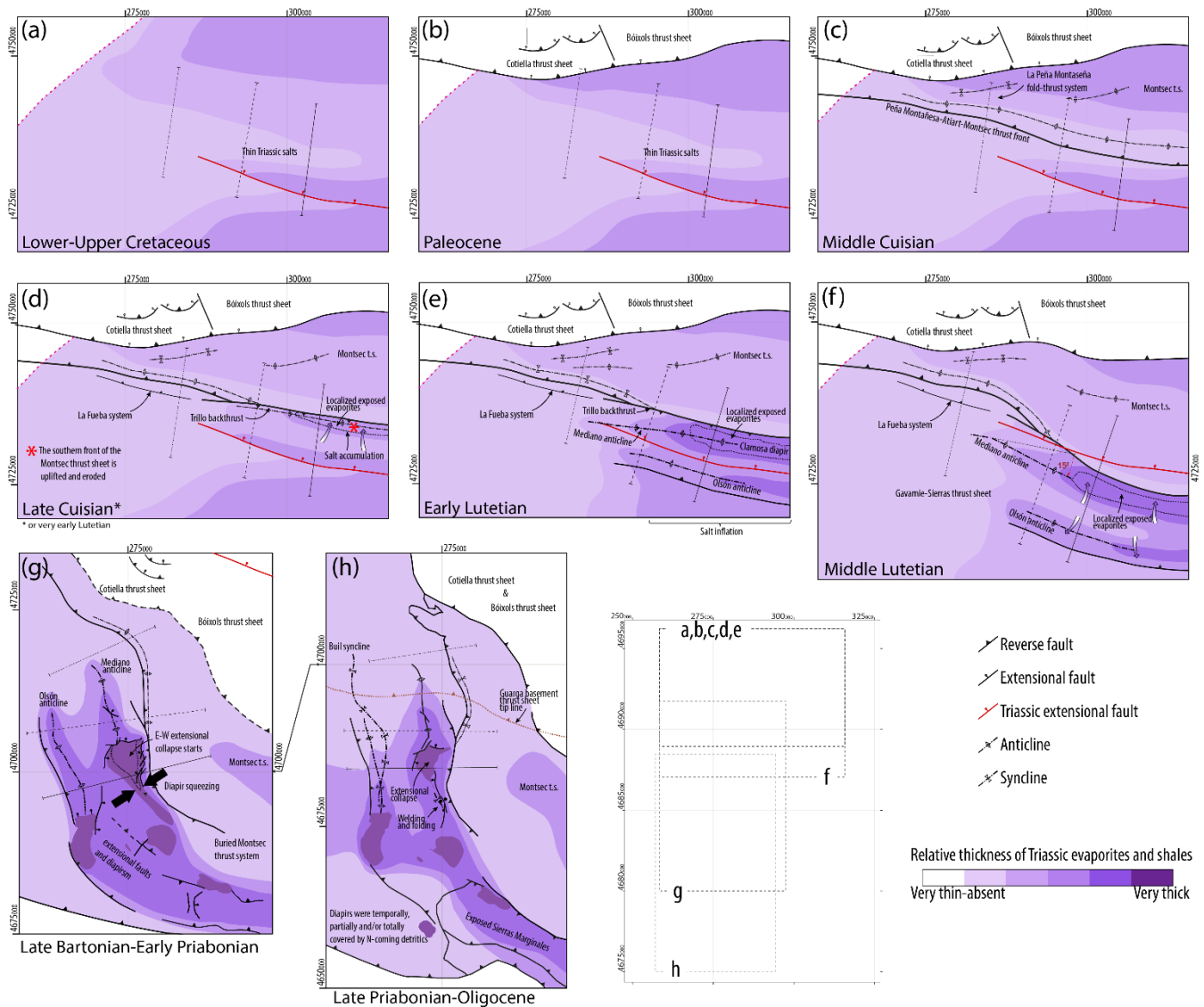
Figure 10. Plan view reconstruction of the studied area (partly modified from Muñoz et al., 2013 and Santolaria et al., 2014). Weak to strong purple denote thin to thick Triassic salt accumulations. Red line represents the basement normal fault bounding the southern salt basin as seen in Fig. 9.

Following the emplacement of the Peña Montañesa-L'Atiart-Montsec thrust system, contractional deformation was transmitted to the southern salt basin and the Trillo backthrust formed (Fig. 9d) as one of the earliest structures related to the deformation

28

of the Gavarnie Sierras thrust sheet. Emplacement of the Trillo backthrust has been dated after foraminifera content. Emplacement postdates the Montsec-Peña Montañesa thrust sheet, since the Trillo backthrusts truncates it, and predates deposition of SBZ12 sediments (see section 3.1, Table 1) found in Salinas de Trillo (Site 1) and Lapenilla (Site 2) villages; these SBZ12 sediments overlay Triassic evaporites and shales (Figs. 7 and 8). This backthrust formed as WNW-ESE structure along the northern edge of the southern salt basin, synchronously with the La Fueba system westward the edge of the southern salt basin (Fig. 10d). Its emplacement involves the truncation of the Montsec thrust whose southern termination was brought upwards, exposed and eroded together with the Gavarnie-Sierras succession. Structural uplift was significant enough to bring up the Triassic evaporites to the surface, as observed and dated in the NE and SE corner of the Clamosa diapir (see biostratigraphic Sites 1 and 2, Fig. 5 and appendix A) where upper Cuisian to earlier Lutetian deposits unconformably overlies Triassic evaporites and shales.

Coeval to soon after the emplacement of the Trillo backthrust, salt inflation took place along the southern salt basin (Fig. 9e, 10e, the nature of inflation is discussed in the following section). Inflation was maximum in the vicinity of the Clamosa diapir and south of it and progressively attenuated to the WNW to finally disappear towards the pinch-out of the Triassic evaporites and shales (Fig. 10e). During the squeezing of the southern salt basin, the Mediano and Olsón anticlines grew (Fig. 9e, 10e). The Mediano anticline registered a peak of uplift during early to middle Lutetian as shown by the stratigraphic record, subsequently decelerating during middle to late Lutetian (Poblet et al., 1998). At that time, the Olsón and specially the Mediano anticline tightened while the syncline in between both deepened into salt (Fig. 9f). Anticline growth occurred synchronous to their vertical axis rotation (Muñoz et al., 2013) while the Clamosa diapir was being squeezed (Fig. 9f, 10f).

During Bartonian-Priabonian times, folding of the Mediano anticline slowed down and halted. At that time the fluvial deposits of the Escanilla Fm. deposited extensively over the area (Fig. 9g). The Escanilla Fm. lies directly on top of Triassic evaporites and shales of the Clamosa diapir suggesting a continuous surficial extrusion of Triassic at that time. This took place synchronously to the southward translation of the Pyrenean thrust sheets that thrust over the Ebro foreland basin deposits (Fig. 9g, 10g). During this event, differential displacement triggered a second phase of clockwise vertical axis rotation that lasted from Priabonian to Chattian (Muñoz et al., 2013). Differential displacement was partially favoured by the differential closure of the Clamosa diapir, which resulted in welding of the diapir's southern edge (Fig. 10h). Later on, during Late Priabonian and Oligocene, crestal collapse of the Clamosa diapir occurred (Fig. 9h). This Late Eocene to Oligocene diapir collapse is evidenced by i) N-S extensional faulting into the diapir in the eastern and western flanks where the Escanilla Fm. and Oligocene conglomerates are deposited on the hanging wall of these faults and ii) north-directed normal faulting of the Bruis syncline where the Escanilla Fm. and Oligocene conglomerates filled a localized depocenter north of Trillo town.

5. Discussion

Despite diapirism is less common in contractional settings than in extensional ones (i.e., Vendeville and Jackson, 1992; Jackson and Vendeville, 1994) it is also a remarkable feature in many fold-and-thrust belts. Those that incorporate and deform pre-shortening early salt structures in rift to rifted margins settings (e.g., Granado et al. 2021, 2023; Santolaria et al. 2021; 2022) usually display a larger budget of salt and salt-related features, such as the Fars province of the Iranian Zagros (Jahjani et al. 2009; Snidero et al. 2020) or the Persian Gulf (Perotti et al. 2016; Snidero et al. 2020), the Northern Calcareous Alps of Austria (Granado et al. 2019; Strauss et al. 2023; Fernández et al. 2024) or), the Betic Cordillera of Spain (Escosa et al., 2018; Flinch and Soto, 2022; Canova et al., 2025), the sub-alpine fold-thrust belt of Haute Provence (Graham et al., 2012) or the North Pyrenean Zone (e.g. Teixell et al., 2016; Espurt et al., 2019).

Salt is easily mobilized upon contraction. Due to its viscous behaviour, shortening of salt horizons entail their immediate redistribution by generalised thickening. Yet, diapirism in contractional systems with no inherited salt structures is commonly hampered by several factors, fundamentally the strengthening of the sedimentary overburden by thickening, either by means of thrust stacking, syn-contractional sedimentation or both. However, salt inflation, overburden piercing and salt extrusion to the syn-orogenic surface can happen when a series of factors coalesce. So, diapir-favouring processes in fold-and-thrust belts include: a thin and weak sedimentary overburden, either pre-existent, or developed by other means, such as by erosion, faulting, restricted sedimentation on top of inflated salt bodies, or combinations of these. Erosion and faulting of thrust wedges and related folds can happen by emergent thrusting and thrust stacking, amplification of detachment folds and formation of fold-accommodation faults (e.g., Coward and Stewart, 1995; Sans and Koyi, 2001; Santolaria et al. 2015; Mitra, 2002; Rowan, 2020). A mobile salt detachment thicker than its sedimentary overburden will strongly favour diapir-formation as well, particularly in combination with the above-mentioned elements. Some of these factors coalesce in the Clamosa diapir, being inflation of the Triassic evaporitic horizon during early Lutetian one of the keystone ones. Salt inflation is inferred after the structural uplift of the Jurassic to early Cuisian succession observed in the Gavarnie-Sierras thrust sheet as registered by the basal Lutetian unconformity (Fig. 9E9e). Such uplift mainly resulted from shortening of the southern Triassic basin. It can be argued that salt might come from the east, but this was also an area of inflation at that time; or from the west as proposed by Holl and Anastasio (1993), but there is no evidence of salt withdrawal structures or growth strata currently north of the Clamosa diapir (west in Lutetian times); or from the north, from the Montsec thrust sheet as proposed by Santolaria et al. (2016), since there was no across-strike connection of the northern and the southern Triassic basins. So, we propose that salt inflation resulted from the thickening of the Triassic salts of the southern Triassic basin due to the displacement of the Montsec thrust front to the SSW. The Montsec thrust front acted as a buttress that embedded into salt while preventing it to migrate northwards.

Balance between favourable and unfavourable factors during mountain building is sensitive to subtle changes that may enhance or halt the formation of diapirs. In their seminal work, Sans and Koyi (2001) propose erosion of anticlines rising to the top free

540   surface increases differential loading on the underlying décollement salt layer and thins and weakens their overburden, promoting diapirism without any change in the dominant contractional tectonic regime. In a simplistic 2d approach of a contractional system, detachment anticlines increase the cross-sectional area during the early stages of development (i.e., Poblet et al., 1998) to allow salt flow towards their cores, while erosion has to be sufficiently deep-reaching for salt to pierce its overburden. As shown for an Appalachians case by Wiltschko and Chapple (1977), open detachment folds with interlimb

545   angles >70° allow salt to accumulate in their cores, whereas fold tightening conversely will promote backflow into the underlying source layer. Since detachment folds need syn-contractional sedimentation to amplify and grow (Poblet et al. 1998), the synclinal troughs adjacent to growing anticlines are depositional sites that sink below the regional level by evacuating salt from the underlying décollement (Mitra, 2003~~).~~), as it has been interpreted for the syncline between the Mediano and Olsón anticlines (compare Fig. 9e and f) . In the crestal area the salt/overburden thickness ratio is greater than both the initial ratio

550   and that under the synclinal troughs. Sedimentation rate must be lower than uplift rate for the growing detachment anticline to keep the hinge zone accessible for erosion (i.e., uplift rate lowers towards the final stages of fold growth by limb rotation; Poblet and Hardy, 1995; Poblet, 2004). When erosion thins or removes the hinge zones of salt-cored anticlines, the resulting differential loading with the adjacent synclinal troughs promotes salt flow inwards and toward the lower pressure core and hinge zone of the anticline. Then, piercing can take place when a critical overburden thickness is reached.

555

Some of these diapirism triggers have been invoked in the Eastern Romanian Carpathians fold-and-thrust belt, where the so-called Moreni-Baicoi "salt lineament" constitutes a 30 km long squeezed diapir (i.e., Schleder et al., 2019; Tămaş et al. 2021). The formation of such salt diapir, aligned with the dominant NE-SW striking structural grain of the fold-and-thrust belt must have been ~~favored~~favoured by some kind of overburden weakening process or processes, since salt *per se* cannot pierce trough

560   the reported c.2-3km thick overburden originally burying the feeding salt horizon. In this sense, local extensional faulting in the transition from frontal to lateral thrust ramps was proposed by Munteanu et al. (2018), which is a plausible mechanism in the lateral terminations of arcuate thrust salients, such as that of the South-Central Pyrenees (Muñoz et al. 2013, 2024). Alternatively, Stefanescu et al. (2000) proposed that a middle-to-late Miocene (i.e., Meotian–Pontian in the local Para-Tethyan chronostratigraphy) extensional phase allowed for salt extrusion to the paleosurface. More recently, Schleder et al. (2019)

565   propose that a large erosional phase in between shortening phases (the large basal Meotian unconformity) deeply eroded the structural culminations of salt-cored detachment anticlines, allowing for the salt rise and flare onto the synorogenic paleosurface. These authors argue that no clear evidence for such phases of regional extension and thick-skinned left-lateral slip are present, as proposed by Stefanescu et al (2000~~). The~~), while the last ~~deformations~~deformation phase~~, according to these authors,~~ rejuvenated and squeezed Carpathian salt structures.

570

Another interesting place for understanding the formation of purely contractional diapirs is the Sureste basin in the Gulf of Mexico (Sánchez Rivera et al. 2011; Davison, 2020). The Sureste basin displays one of the best examples of salt diapirs associated with contraction structures in a deep-water setting, with some salt-detached anticlines reaching astounding structural reliefs of more than 10km (e.g., Rowan et al. 2022). Large erosional peneplanations under deep water conditions are highly unlikely in comparison to onshore shortening systems, and other processes must be responsible for diapirism to occur. In this area, the 3D interaction between detachment folding, thrust faulting, and salt diapirism is exceptionally constrained by seismic data and the key question is whether the salt diapirs predated the shortening or broke out during the contractional deformation. In their reported interpreted seismic sections, the hinges of upright detachment folds are thinned by extensional faults (Rowan et al. 2022) where some of these crestal extensional faults are conjugate and dip inwards in opposite senses, indicating outer arc extension accommodating concentric folding. Laterally, these faults pass into a series of listric convex upwards extensional faults, suggesting extensional collapse of the anticline's crest as reported for other deep-water gravity driven fold-belts (Morley, 2009). The interaction of detachment folding with thrusting and extensional collapses are the main cause for the extrusion of salt a surface since large erosional events are highly unlikely.

In our Pyrenean scenario, an additional process has contributed fundamentally ~~in~~to the formation and evolution of the Mediano anticline and the Clamosa diapir. Beside erosion, localized extensional faulting has also promoted thinning of the overburden. The youngest structures are extensional faults (Teixell and Barnolas, 1995; Fernández, 2004) with a variable trend from N–S to E–W. The most prominent one has a curvilinear map pattern and a throw of about 1 km that cuts the Montsec-Peña Montañesa thrust sheet and the Gavarnie thrust sheet below (the Balupor-San Marzial fault; Fernández, 2004). Extensional faults of this system obliquely truncate several anticlines of the Aínsa oblique zone and are spatially associated with extensive Triassic outcrops~~.~~ (Muñoz et al., 2013). In cross section, these extensional faults appear as collapse features of the anticlines as they partially reactivate their related thrusts at depth (e.g., Tavani et al. 2006). Since these extensional faults control along-strike changes in the geometry of anticlines their occurrence suggests some synchronicity with fold growth (Fernández et al., 2012) and are known to be active at least until Priabonian times since these faults offset late Eocene sediments. The extensional faults defining the ~~southern~~ boundary ~~of~~between the Mediano anticline-Bruis syncline and the Clamosa diapir are similar in nature to the Balupor-San Marzial fault in that they both are interpreted to be contained entirely within the Gavarnie thrust sheet. The extensional faults are active until the Oligocene at least, since they cut through sediments of that age, and crosscut the entirety of the Mediano anticline. Furthermore, the Balupor-San Marzial and the Clamosa faults are located where the N–S striking Aínsa oblique structures swing to a NW–SE trend northwards in the case of the Balupor-San Marzial and southwards in the case of Clamosa.

The origin of these extensional features relates to the contractional phase concomitant with the clock-wise vertical axis rotation of the Aínsa Oblique Zone (Fig. 4). Paleomagnetic data from the N–S trending structures of the Aínsa Oblique Zone reveals the kinematics of the South-Central Pyrenees thrust salient (Mochales et al., 2012, Muñoz et al., 2013). These structures

605   experienced clockwise vertical axis rotations that vary from 70° in the Mediano anticline to 55° further to the west. Rotations of about 60°-45° occurred from early Lutetian to late Bartonian when the Clamosa diapir and Mediano anticline developed. Rotation was partially accommodated by squeezing of a salt inflated area, the oblique to strike-slip reactivation of former thrusts, and by the formation of new extensional faults, all these contributing to the thinning of the overburden and diapirism, as indicated by the spatial association of these faults to outcrops of Triassic evaporites. In the case of the Mediano anticline,

610   rotation progressively diminished as recorded by its growth strata. Starting during the early Lutetian, the decrease in the amount of rotation has been observed from 47.5 Ma onward. Syn-folding rotation continued at a decreasing rate at least into the Priabonian. This vertical axis rotation stage resulted from a difference of about 50 km in the amount of displacement on the Gavarnie thrust and an accompanying change in structural style at crustal scale from the central to the western Pyrenees. Such change has been interpreted originally as related to the NE–SW trending pinch out of Triassic evaporites at its basal (Muñoz

615   et al. 2013), and has been recently tested as well by means of sandbox analogue models (Muñoz et al. 2024).

Finally, during Priabonian to Oligocene the crest of the Clamosa diapir collapsed. In contractional settings and regardless if pre-existing or newly formed diapirs exist, they are prone to be squeezed and finally welded. It is at this point when crestal collapse may occur. Squeezing of a diapir leads to the creation of an active summit dome that eventually collapse when it

620   disconnects from the salt feeder, or squeezing stops (commonly by secondary welding) (e.g. Santolaria et al., 2021). Crestal collapse is a phenomenon that takes place locally, involving just the crest of the diapir. There salt flows and readjusts creating local extension and salt extrusions. Evidence of this is the topographic distribution of Triassic salt in the Clamosa diapir where nowadays top of Triassic salt is located few hundreds meters above the base of the collapse-related Oligocene sequence.

625   **6. Conclusions**

The northwestern termination of the South-Central Pyrenean Salient serves as an outstanding scenario that exemplifies the evolution of purely contractional diapirs. First, syn-growth sediments provide an excellent dating tool for deciphering the structural evolution within areas tens of kilometres wide. As discussed, the formation of the Clamosa diapir responds to a

630   combination of multiple factors that can be taken as a rule of thumb for diapir initiation and evolution within contractional settings. These include: the occurrence of a thick salt accumulation relative to isits sedimentary overburden previous to the onset of shortening, the inflation of it upon shortening and a series of concomitant processes that thin this overburden to the point that salt can pierce through it. These can be folding, uplift, and thinning of the overburden, either produced by erosion or local extensional faulting. related first to the vertical axis rotation of the western termination of the South Pyrenean Central

635   Salient and later by the crestal collapse of the diapir. Conversely, in the La Fueba system 15 km to the north of the Clamosa diapir, thin or absent salt, thrust stacking and moderate to high syncontractional sedimentation led to the formation of a contractional thrust system instead. The Mediano anticline could be considered as an intermediate member in which salt accumulated in its core, but erosion was not significant enough to expose it. All in all, our emplacement and growth model for

33

the Clamosa diapir, the Mediano anticline and the La Fueba thrust system illustrates how along strike changes in salt and cover thicknesses, thrust stacking and erosion-sedimentation processes lead to lateral variations that may trigger or hinder diapirism in contractional settings. Examples from other contractional settings such as the Eastern Romanian Carpathians and the Sureste basin of Mexico suggest a key role of regional erosional episodes in the flaring and extrusion of salt from the cores of detachment anticlines, or the extensional faulting to accommodate folding, or due to gravitational collapses of hinges and flanks in promoting diapirs under contraction regimes.
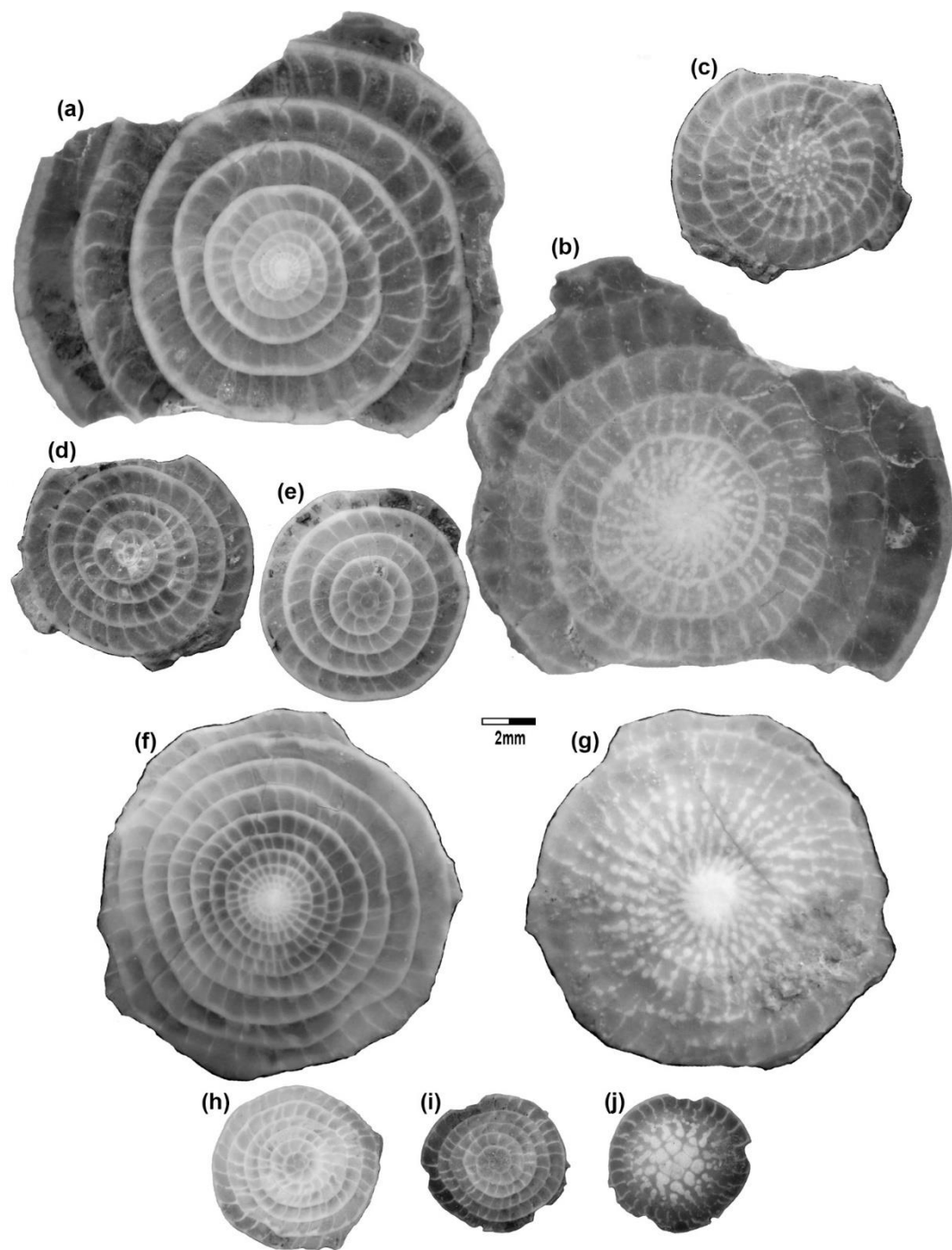
645

FIGURE A1

FIGURE A2

2mm
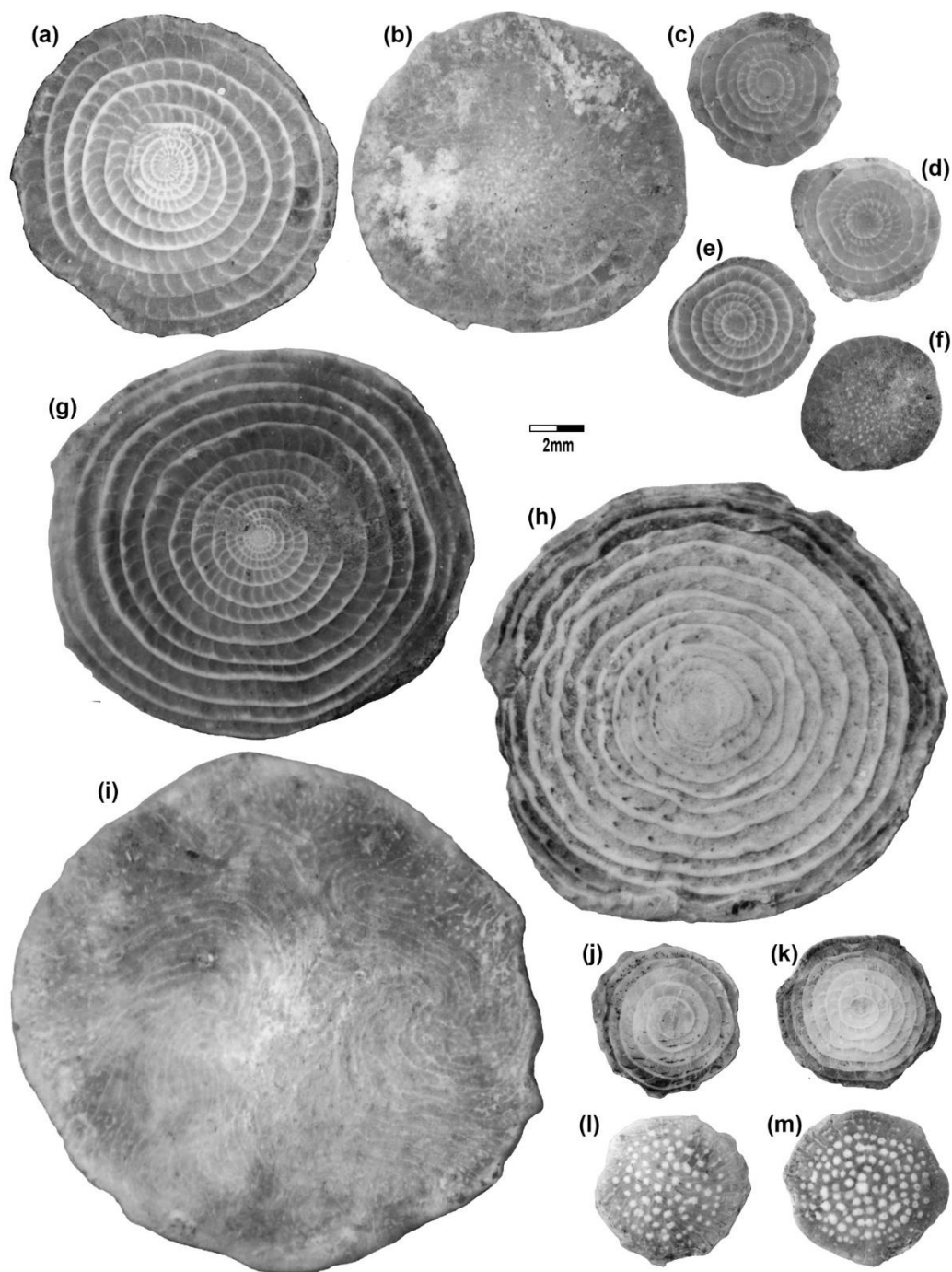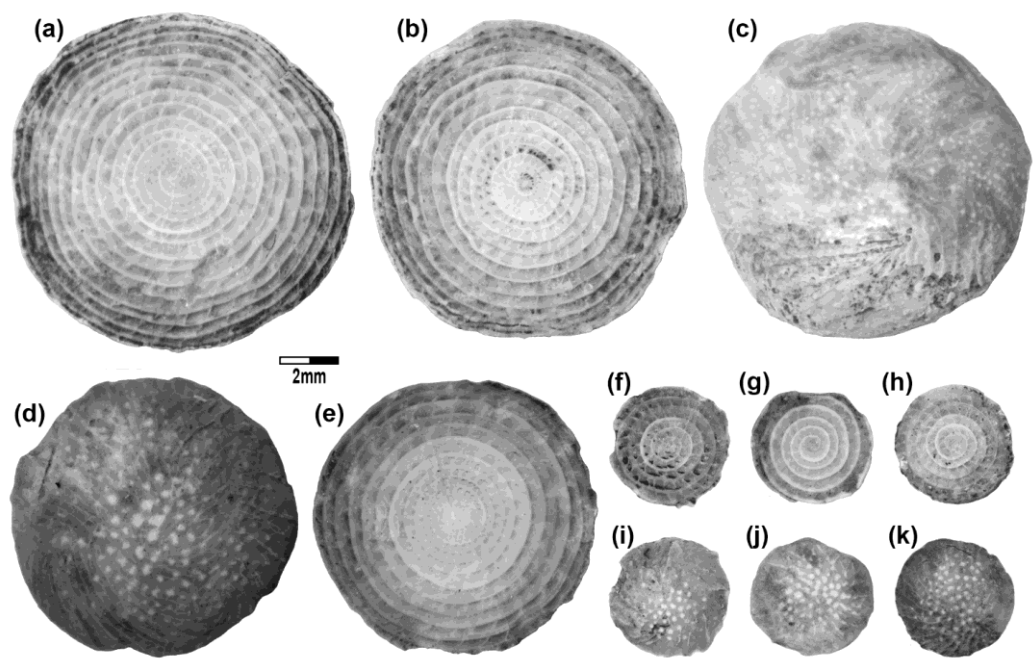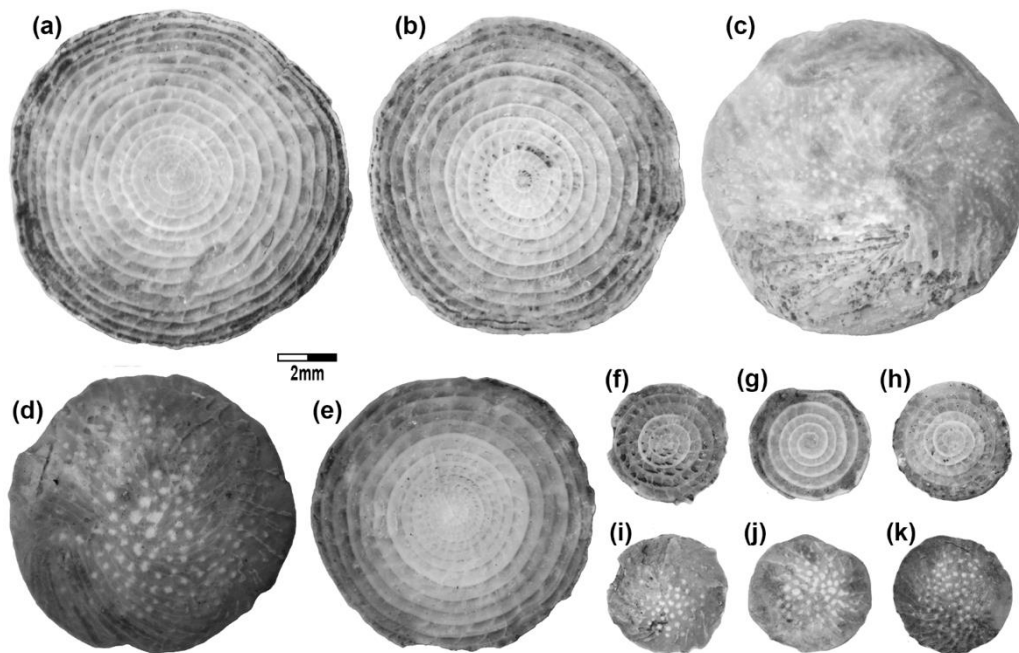
FIGURE A3

Figure captions:

Fig. A1: *Assilina maior* (a – e) and *A. cuvillieri* (f – j) a) *A. maior,* B form, equatorial section. b) *A. maior*, B form, external view. c) *A. maior,* A form, external view. d) and e) *A. maior,* A form, equatorial section. f) *A. cuvillieri*, B form, equatorial section. g) *A. cuvillieri*, B form, external view. h) and i). *A. cuvillieri*, A form, equatorial section. j) *A. cuvillieri*, A form, external view. All samples from **sample ST-1**. All samples 5x.

Fig. A2: *Nummulites manfredi* (a - f) and *N.* aff. *boussaci* (g - m). a) *N. manfredi,* B form, equatorial section. b) *N. manfredi,* B form, external view. c) and e) *N. manfredi,* A form, equatorial sections. f) *N. manfredi,* A form, external view. g) and h): *N.* aff. *boussaci,* B form, equatorial sections. (i): *N.* aff. *boussaci,* B form, external view. j) and k) *N.* aff. *boussaci,* A form, equatorial sections. l) and m) *N.* aff. *boussaci,* A form, external views. **Samples a) – f)** from **sample LP-1**, **samples g) – m)** from **sample Cb-4**. All samples 5x.

Fig. A3: *Nummulites campesinus.* a) and b) *N. campesinus,* B form, equatorial sections. c) and d) *N. campesinus,* B form, external views. d) *N. campesinus,* B form, equatorial section. f – h) *N. campesinus,* A forms, equatorial sections. i – k) *N. campesinus,* A form, external views. **All samples** from **sample ST-1**. All samples 5x.

8. Appendix B. Uninterpreted version of seismic lines
FIGURE B1

38
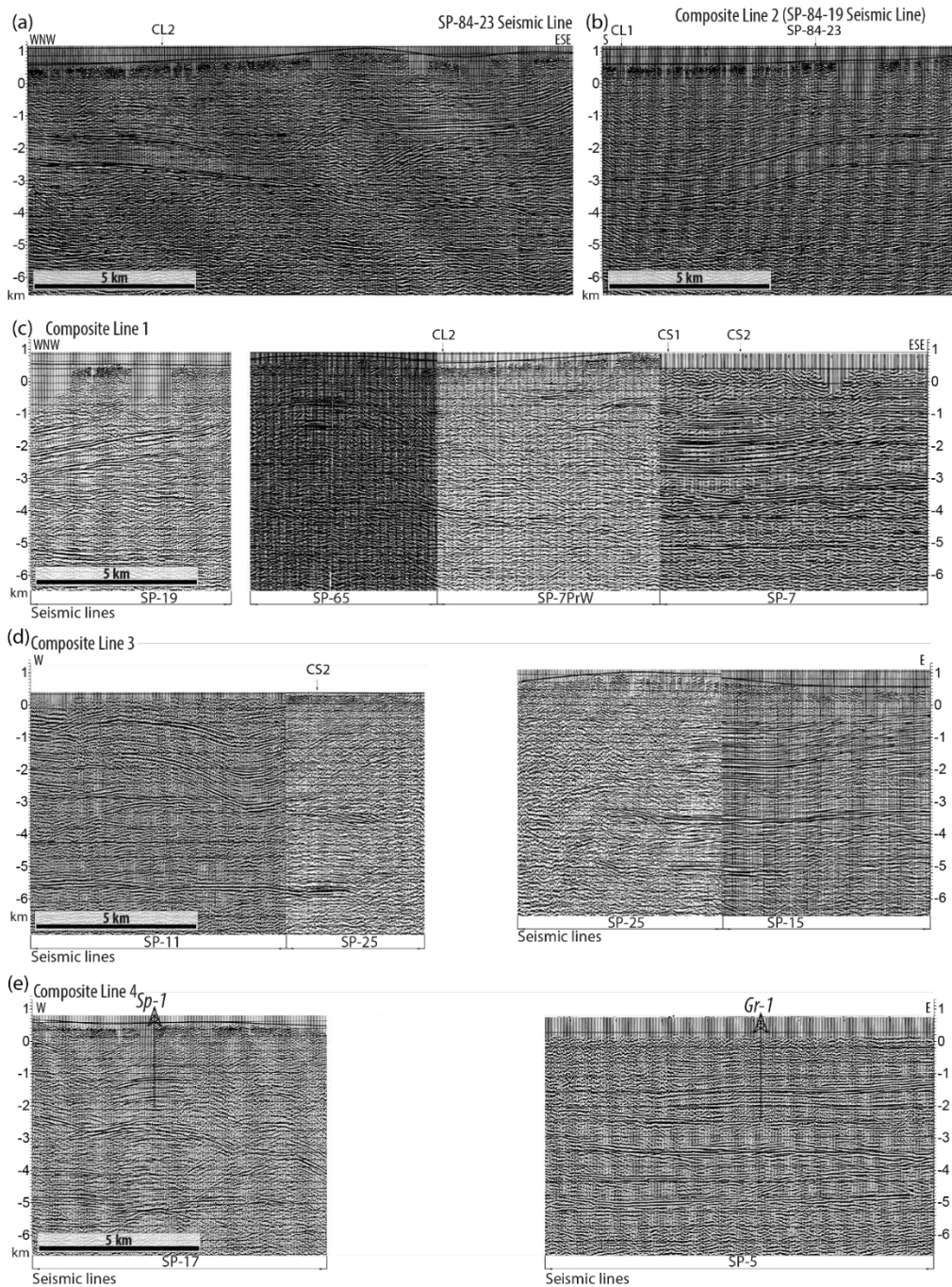
Fig. B1: Uninterpreted version of (a) SP-84-23 seismic line, (b) SP-84-19 seismic line (part of the Composite Line 2, see fig. 8 in the main text), (c) SP-19, SP-65, SP-7PrW and SP-7 seismic lines (Composite Line 1, see fig. 7 in the main text), (d) SP-11, SP-25 and SP-15 (Composite Line 3, see fig. 8 in the main text) and (e) SP-17 and SP-

5 (Composite Line 4, see fig. 8 in the main text). Surpireanica-1 and Graus-1 exploration wells are labelled as Sp-1 and Gr-1 respectively. Intersections between seismic lines or cross-sections are indicated with regular, capital characters on top of vertical arrows; labels CL-1, CL2, CL-3, CS-1 and CS-2 correspond to Composite Line 1, Composite Line 2, Composite Line 3, Cross Section 1 and Cross Section 2 respectively (as in the main text).

685

Data Availability Statement

Seismic reflection profiles for this research are available and freely accessible in the SIGEOF repository, the Geophysical Information System of the IGME (Spanish Geological Survey). To access the data, use the web application (info.igme.es/SIGEOF/).

690

Author contribution

P.S.: Conceptualization, Methodology, Formal analysis, Investigation, Writing - Original Draft, Writing - Review & Editing

R.S.: Methodology, Formal analysis, Investigation, Writing - Review & Editing

N.C.: Formal analysis, Investigation, Writing - Review & Editing

695 J.AM.: Conceptualization, Formal analysis, Project administration, Writing - Review & Editing

P.A.: Formal analysis, Investigation, Writing - Review & Editing

P.G.: Writing - Review & Editing

Competing interest

700 The authors declare that they have no conflict of interest.

Acknowledgements

705 **References**

Arbués, P., D. Mellere, O. Falivene, O. Fernández, J. A. Muñoz, Marzo, M. and de Gibert, J. M., (2007). Context and architecture of the Ainsa-1-quarry channel complex, Spain, in T. H. Nilsen, R. D. Shew, G. S. Steffens, and J. R. J. Studlick, eds., Atlas of deep-water outcrops: AAPG Studies in Geology 56, CD-ROM, 20 pp.

Barnolas, A., Samsó, J. M., Teixell, A., Tosquella, J. and Zamorano, M., (1991). Evolución sedimentaria entre la cuenca de
710 Graus-Tremp y la cuenca de Jaca-Pamplona, in Colombo, F., ed., I Congreso el Grupo Español del Terciario: Libro-Guía de la Excursión 1: EUMO ~~Gràfi e~~Gràfic, Vic, Spain, 123 pp.

~~Barnolas, A., Teixell, A., García Senz, J., and Ramirez, J. I., (1994a). Mapa Geológico de España. 1:50000, Hoja 288, Fonz, IGME.~~

~~Barnolas, A., Teixell, A., Zamorano, M. and Ramirez, J. I., (1994b). Mapa Geológico de España. 1:50000, Hoja 250, Graus,~~
715 ~~IGME.~~

~~Barnolas, A., Robador Moreno, A., Zamorano, M. (1999). Mapa Geológico de España. 1:50000, Hoja 212, Campo, IGME.~~

Barrier, L., Nalpas, T., Gapais, D. and Proust, J. N., (2013). Impact of synkinematic sedimentation on the geometry and dynamics of compressive growth structures: Insights from analogue modelling. Tectonophysics 608, 737-752.

Beamud Amorós, E. (2013). Paleomagnetism and thermochronology in tertiary syntectonic sediments of the south-central Pyrenees: chronostratigraphy, kinematics and exhumation constraints. Tesis Doctoral, Univ. Barcelona, 251 pp.

Bentham, P. A. and Burbank, D. W. (1996). Chronology of Eocene foreland basin evolution along the western oblique margin of the South-Central Pyrenees, in Tertiary basins of Spain, edited by P. F. Friend and C. J. Dabrio, Cambridge University Press, 144-152.

Bonini, M. (2003). Detachment folding, fold amplification, and diapirism in thrust wedge experiments. Tectonics 22, 1065-1103.

Burrel, L., & Teixell, A. (2021). Contractional salt tectonics and role of pre-existing diapiric structures in the Southern Pyrenean foreland fold–thrust belt (Montsec and Serres Marginals). Journal of the Geological Society, 178(4). https://doi.org/10.1144/jgs2020-085

Callot, J. P., Trocmé, V., Letouzey, J., Albouy, E., Jahani, S. and Sherkati, S. (2012). Pre-existing salt structures and the folding of the Zagros Mountains. In, Alsop, G. I., Archer, S. G., Hartley, A. J., Grant, N. T. and Hodgkinson, R. (eds) 2012. Salt Tectonics, Sediments and Prospectivity. Geological Society, London, Special Publications 363, 545–561. http://dx.doi.org/10.1144/SP363.27

Calvín, P., Casas-Sainz, A.M., Villalaín, J.J., Moussaid, B., 2018. Extensional vs. compressional deformation in the Central High Atlas salt province: a paleomagnetic approach. Tectonophysics 130–147. https://doi.org/10.1016/j.tecto.2018.04.007, 734–735.

Cámara, P. and Klimowitz, J. (1985). Interpretación geodinámica de la vertiente centro-occidental surpirenaica (Cuencas de Jaca-Tremp). Estudios geológicos 41, 391-404.

Campanyà, J., Ledo, J., Queralt, P., Marcuello, A., Liesa, M. and Muñoz, J. A. (2012). New geoelectrical characterisation of a continental collision zone in the West-Central Pyrenees: Constraints from long period and broadband magnetotellurics. Earth and Planetary Science Letters 333-334, 112-121

Canérot, J., Hudec, M.R., Rockenbauch, K., 2005. Mesozoic diapirism in the Pyrenean orogen: Salt tectonics on a transform plate boundary. AAPG Bulletin, 89, 211-229.

Canova, D.P., Roca, E., Ferrer, O., Ferràndez-Cañadell, C., Escosa, F.O., Afzal, J., 2025. From salt carapace to secondary minibasin encasement—The Bolon Secondary Minibasin, Eastern External Betics SE Iberia. https://dx.doi.org/10.2139/ssrn.5095927

Casas-Sainz, A.M., Villalaín. J.J., Román-Berdiel, T., Calvín, P., Marcén, M., Izquierdo-Llavall, E., Santolaria, P., Pocoví, A., Mochales, T., Oliva-Urcia, B., El-Ouardi, H., Moussaid, 2023. Structure of the Central High Atlas (Morocco). Kinematics of Structures and Basin Evolution in the Central High Atlas. Constraints from AMS and Paleomagnetic Data. In: Tectonic Evolution of the Moroccan High Atlas: A Paleomagnetic Perspective, eds. Calvín, P., Casas-Sainz, A.M., Román-Berdiel, T., Villalaín, J.J., Springer Geology, pp. 487-646.

Casini, G., Vergés, J., Drzewiecki, P., Ford, M., Cruset, D., Wright, W., & Hunt, D. (2023). Reconstructing the Iberian salt-bearing rifted margin of the southern Pyrenees: Insights from the Organyà Basin. Tectonics, 42(7), e2022TC007715. https://doi.org/10.1029/2022TC007715

Célini, N., Callot, J.-P., Ringenbach, J.-C., Graham, R., 2020. Jurassic salt tectonics in the SW sub-alpine fold-and-thrust belt. Tectonics 39 (10). https://doi.org/10.1029/2020TC006107, 47–36.

Chevrot, S., Sylvander, M., Díaz, J., Martin, R., Mouthereau, F., Manatschal, G., Masini, E., Calassou, S., Grimaud, F., Pauchet, H. and Ruiz, M. (2018). The non cylindrical crustal architecture of the Pyrenees. Scientific Reports 8(1), 9591pp. http://doi.org/10.1038/s41598-018-27889-x

Chevrot, S., Sylvander, M., Diaz, J., Ruiz, M., Paul, A. and the PYROPE Working Group (2015) The Pyrenean architecture as revealed by teleseismic P-to-S converted waves recorded along two dense transects. Geophysical Journal International, 200(2), 1094–1105. doi:10.1093/gji/ggu400

Choukroune, P., (1989). The ECORS Pyrenean deep seismic profile reflection data and the overall structure of an orogenic belt. Tectonics 8 (1), 23-39.

Costa, E., and Vendeville, B. C. (2002). Experimental insights on the geometry and kinematics of fold-and-thrust belts above a weak, viscous evaporite décollement. Journal of Structural Geology 24 (11), 1729-1739.

Cotton, J. T. and Koyi, H. A. (2000). Modeling of thrust fronts above ductile and frictional detachments: Application to structures in the Salt Range and Potwar Plateau, Pakistan. Geol. Soc. Amer. Bull. 112, 351-363.

Davis, D. M. and Engelder, T. (1985). The role of salt in fold and thrust belts and accretionary wedges: cohesive Coulomb theory. Journal of Geophysical Research, 89, 10087-10101.

Davison, I., 2020. Salt tectonics in the Sureste Basin, SE Mexico: some implications for hydrocarbon exploration. In: Davison, I., Hull, J.N.F., Pindell, J. (Eds.), The Basins, Orogens and Evolution of the Southern Gulf of Mexico and Northern Caribbean. Geol. Soc., vol. 504 Spec. Pub, London. https://doi.org/10.1144/SP504-2019-227.

De Federico, A., (1981). La sedimentación de talud en el sector occidental de la cuenca paleógena de Ainsa: Bellaterra, Universitat Autònoma de Barcelona, Publicacions de Geologia, v. 12, 271 p.

De Ruig, M.J., 1995, Extensional Diapirism in the Eastern Prebetic Foldbelt, Southeastern Spain: M.P.A. Jackson, D.G. Roberts, and S. Snelson, eds., Salt tectonics: a global perspective: AAPG Memoir 65, p. 353–367

Dooley, T.P., Jackson, M.P.A., Hudec, M.R., 2009. Inflation and deflation of deeply buried salt stocks during lateral shortening. J. Struct. Geol. 31, 582–600. https://doi. org/10.1016/j.jsg.2009.03.013.

Duerto, L. and McClay, K. (2009). The role of syntectonic sedimentation in the evolution of doubly vergent thrust wedges and foreland folds. Marine and Petroleum Geology 26(7), 1051–1069.

Escosa, F.O., Roca, E., Ferrer, O., 2018. Testing thin-skinned inversion of a prerift salt-bearing passive margin (Eastern Prebetic Zone, SE Iberia). Journal of Structural Geology, 109, 55-73.

Espurt, N., Angrand, P., Teixell, A., Labaume, P., Ford, M., de Saint Blanquat, M., Chevrot, S., 2019. Crustal-scale balanced cross-section and restorations of the Central Pyrenean belt (Nestes-Cinca transect): highlighting the structural control of

785   Variscan belt and Permian-Mesozoic rift systems on mountain building. Tectonophysics 764, 25–45.

Fernández, O., Muñoz J. A., Arbués, P. and Falivene, O. (2012). 3D Structure and evolution of an oblique system of relaying folds: The Ainsa basin (Spanish Pyrenees). Journal of the Geological Society of London 169, 545-559.

Fernández, O., Muñoz, J. A., Arbués, P., Falivene, O., Marzo, M. (2004). Three-dimensional reconstruction of geological

790   surfaces: An example of growth strata and turbidite systems from the Ainsa basin (Pyrenees, Spain). AAPG Bulletin, 88(8), 1049-1068.

Fernández-Bellón, O. (2004). Reconstruction of geological structures in 3D. An example from the Southern Pyrenees. Ph.D. thesis, Universitat de Barcelona, 321 pp.

Fernández, O., Ortner, H., Sanders, D., Grasemann, B., Leitner, T., 2024. Salt-rich versus salt-poor structural scenarios in the

795   central Northern Calcareous Alps: implications for the Hallstatt facies and early Alpine tectonic evolution (Eastern Alps, Austria). International Jorunal of Earth Sciences, https://doi.org/10.1007/s00531-023-02377-4

Fillon, C., Huismans, R. S., van der Beek, P. and Muñoz, J. A. (2013). Syntectonic sedimentation controls on the evolution of the southern Pyrenean fold-and-thrust belt: Inferences from coupled tectonic-surface processes models. Journal of geophysical research: Solid Earth, 118, 1-16.

800   Flinch, J.F., Soto, J.I. (2022). Structure and Alpine tectonic evolution of a salt canopy in the western Betic Cordillera (Spain). Marine and Petroleum Geology 143, 105782, https://doi.org/10.1016/j.marpetgeo.2022.105782.

Franco-Balaguer, J., Casas Sainz, A.M. (2016): Estructura de la terminación occidental del cabalgamiento del Montsec (Pirineos Centrales). Revista de la Sociedad Geológica de España, 29(2): 39-55.

Garrido-Megías, A. (1968). Sobre la estratigrafía de los conglomerados de Campanué (Santa Liestra) y formaciones superiores

805   del Eoceno (extremo occidental de la cuenca de TrempGraus, Pirineo central, provincia de Huesca). Acta. Geol. Hispánica, 3, pp. 39-43.

Garrido-Megías, A. (1973). Estudio geológico y relación entre tectónica y sedimentación del Secundario y Terciario de la vertiente meridional pirenaica en su zona central (Provincias de Huesca y Lérida). PhD thesis, Universidad de Granada, 395pp.

Garrido-Megías, A., Rios-Aragües, L.M. (1972). Síntesis geológica del Secundario y Terciario entre los ríos Cinca y Segre

810   (Pirineo central de la vertiente sur pirenaica, provincias de Huesca y Lérida). Boletín Geológico y Minero, 83, 1-47.

Gomis, L. E., López-Blanco, M., Vidal, I. and Serra-Kiel, J. (2012). Arquitectura y distribución de sedimentos marinos someros y de talud influenciados por el crecimiento de pliegues sinsedimentarios (Abizanda, Luteciense medio, Zona Surpirenaica Central). VIII Congreso Geológico de España. Geo-Temas 13, 106.

Gradstein, F.M., Ogg, J.G., Schmitz, M.D., Ogg, G.M., 2020. Geologic Time Scale 2020. Elsevier, 1357pp,

815 https://doi.org/10.1016/C2020-1-02369-3

Graham, R., Jackson, M., Pilcher, R., & Kilsdonk, B. (2012). Allochthonous salt in the subAlpine fold–thrust belt of Haute Provence, France. In Salt tectonics, sediments and prospectivity. *Geological Society, London, Special Publications*, *363*(1), 595–615. https://doi.org/10.1144/SP363.30

820   Granado, P., Santolaria, P., Muñoz, J.A., 2023 Interplay of downbuilding and gliding in salt-bearing rifted margins: insights from analogue modelling and natural case studies. AAPG Bulletin, 107, 12, 2091-2118, DOI:10.1306/08072221203.

Granado, P., Roca, E., Strauss, O., Pelz, K., Muñoz, J.A. (2019). Structural styles in fold-and-thrust belts involving early salt structures: The Northern Calcareous Alps (Austria). Geology 47(1), 51-54. doi: 10.1130/G45281.1

Granado, P., Ruh, J.B., Santolaria, P., Strauss, P., Muñoz, J.A. (2021). Stretching and Contraction of Extensional Basins With

825   Pre-Rift Salt: A Numerical Modeling Approach. Frontiers in Earth Science 9, https://doi.org/10.3389/feart.2021.648937

Harrison, J. C. (1995). Tectonics and kinematics of a foreland folded belt influenced by salt, Arctic Canada. In M. P. A. Jackson, D. G. Roberts, and S. Snelson, eds., Salt tectonics: a global perspective. AAPG Memoir 65, 379-412.

Heim, A. (1908). Die Nummuliten- und Flyschbildungen der Schweizeralpen, Versuch zu einer Revision der alpinen Eocaen-Stratigraphie. Abhandlungen Der Schweizerischen Paläontologischen Gesellschaft, vol. 35: 1–330

830   Holl, J. E., and Anastasio, D. J. (1993). Paleomagnetically derived folding rates, southern Pyrenees, Spain. Geology 21, 271-274 pp.

Hudec, M.R., Dooley, T.P., Burrel, L., Teixell, A., Fernandez, N., 2021. An alternative model for the role of salt depositional configuration and preexisting salt structures in the evolution of the Southern Pyrenees, Spain. Journal of Structural Geology 146, 104325. https://doi.org/10.1016/j.jsg.2021.104325

835   Izquierdo-Llavall, E., Roca, E., Xie, H., Pla, O., Muñoz, J. A., Rowan, M. G., Yuan, N. and Huang, S. (2018). Influence of Overlapping décollements, Syntectonic Sedimentation, and Structural Inheritance in the Evolution of a Contractional System: The Central Kuqa Fold-and-Thrust Belt (Tian Shan Mountains, NW China). Tectonics, https://doi.org/10.1029/2017TC004928

Jackson, M. P. A. and Vendeville, B. C. (1994). Regional extension as a geologic trigger for diapirism. GSA Bulletin 106, 57–73.

840   Jahani, S., Callot, J. P., Letouzey, J., Frizon De Lamotte, D., 2009. The eastern termination of the Zagros Fold-and-Thrust Belt, Iran: Structures, evolution, and relationships between salt plugs, folding, and faulting. Tectonics, 28 (6), TC6004 doi:10.1029/2008TC002418.

López-Gómez et al., 2019 In: C. Quesada and J. T. Oliveira (eds.), The Geology of Iberia: A Geodynamic Approach, Regional Geology Reviews. Springer Nature Switzerland AG 2019 https://doi.org/10.1007/978-3-030-11295-0_3

845   Martínez-Peña, M. B. and Casas-Sainz, A. M. (2003). Cretaceous-Tertiary tectonic inversion of the Cotiella Basin (Southern Pyrenees, Spain). International Journal of Earth Sciences (Geol. Rundsch.) 92, 99-113.

Martín-Martín, J. D., Vergés, J., Saura, E., Moragas, M., Messager, G., Baqués, V., Razin, P., Grélaud, C., Malaval, M., Joussiaume, R., Casciello, E., Cruz-Orosa, I., Hunt, D.W. (2017). Diapiric growth within an Early Jurassic rift basin: The Tazoult salt wall (central High Atlas, Morocco), Tectonics, 36, 2–32, doi:10.1002/2016TC004300

850   Mateu-Vicens, G., Pomar, L. and Ferrández, C. (2012). Nummulitic banks in the upper Lutetian "Buil level", Ainsa Basin, South Central Pyrenean Zone: The impact of internal waves, Sedimentology 59(2), 527–552.

Mey, P. H. W., P. J. C. Nagtegaal, K. J. Roberti, and J. J. A. Hartevelt (1968). Lithostratigraphic subdivision of post-Hercynian deposits in the south-central Pyrenees, Spain, Leidse Geologische Mededelingen, 431, 221–228

Mitra, S. (2002) Fold-Accommodation Faults. AAPG Bulletin 86 (4), 671–693.

855   Mitra, S. 2003. A unified kinematic model for the evolution of detachment folds. Journal of Structural Geology 25, 1659-1673.

Mochales, T., Casas, A.M., Pueyo, E.L., Barnolas, A., 2012. Rotational velocity for oblique structures (Boltaña anticline, Southern Pyrenees). J. Struct. Geol. 35, 2–16.

Morley, C.K. (2009) Growth folds in a deep water setting. Geosphere 5 (2), 59–89. doi: 10.1130/GES00186.1

Mugnier, J. L., Baby, P., Colletta, B., Vinour, P., Bale, P., Leturmy, P., 1997. Thrust geometry controlled by erosion and 860   sedimentation: a view from analogue models. Geology 25(5), 427-430.

Munteanu I, Garcia A, Dobre S, Tilita M, Vasiliu M, Fernandez O, Matias H, Tulucan A, Cascone L, Escandell F, Garcia Gomez, M (2018) Lateral ramps and salt diapirism in the Diapiric Fold Zone of Romania. AAPG Granada, Workshop 2018

Muñoz, J. A. (1992). Evolution of a continental collision belt: ECORS-Pyrenees crustal balanced cross section. In: Thrust tectonics, (K. R. McClay, ed.), Chapman & Hall, Londres, 235-246.

865   Muñoz, J. A., Beamud, E., Fernández, O., Arbués, P., Dinarès-Turell, J. and Poblet, J. (2013). The Ainsa Fold and Thrust Oblique Zone of the Central Pyrenees: kinematics of a curved contractional system from paleomagnetic and structural data. Tectonics 32(5), 1142-1175.

Muñoz, J. A., Mencos, J., Roca, E., Carrera, N., Gratacos, O., Ferrer, O. and Fernandez, O. (2018). The structure of the South-Central Pyrenean fold and thrust belt as constrained by subsurface data. Geologica Acta: an International Earth Science Journal 870   16(4), 439–460. http://doi.org/10.1344/GeologicaActa2018.16.4.7

Muñoz, J.A., Ferrer, O., Gratacós, O., Roca, R., 2024. The influence of the geometry of salt detachments on thrust salient development: An analogue modelling approach based on the South-Central Pyrenean thrust salient. Journal of Structural Geology, 105078, https://doi.org/10.1016/j.jsg.2024.105078

Nijman, W., Nio, S.D. (1975). The Eocene Montañana delta. In: J. Rosell and Puigdefábregas (Eds.), Sedimentary evolution 875   of the Paleogene South Pyrenean Basin. IAS 9th International Congress, Nice, part B, 56 p.

Nijman, W., Puigdefàbregas, C., 1978. Coarse-grained point bar structure in a molasse-type system, Eocene Castissent Formation, South Pyrenean Basin. In: Fluvial Sedimentology (Ed. A.D. Miall). Mem. Can. Soc. Petrol. Geol., 5, 487-510.

Pedreira, D., Pulgar, J. A., Gallart, J. and Díaz, J. (2003). Seismic evidence of Alpine crustal thickening and wedging from the western Pyrenees to the Cantabrian Mountains (north Iberia). Journal of Geophysical Research: Solid Earth 108(B4), 2204. 880   doi:10.1029/2001JB001667

Pichot, T. and Nalpas, T. (2009). Influence of synkinematic sedimentation in a thrust system with two decollement levels; analogue modelling. Tectonophysics 473, 466-475.

Plaziat, J.C., (1984), Le domaine Pyrénéen de la fin de Crétacé a la fin de l'Eocene. Stratigraphie, paléoenvironments et évolution paléogeographique. PhD Thesis. Université de Paris-sud, 1362p.

885   Poblet, J., Muñoz, J. A., Travé, A. and Serra-Kiel, J. (1998). Quantifying the kinematics of detachment folds using three-dimensional geometry: Application to the Mediano anticline (Pyrenees, Spain). Geological Society of America Bulletin 110(1), 111-125.

Ramirez-Perez, P., Cofrade, G., Martín-Martín, J.D., Travé, A., 2024. Stratigraphic evolution of a salt-walled basin: the influence of diapirism and compressional tectonics on the sedimentary record of the Estopanyà syncline (South-Central

890   Pyrenees). Marine and Petroleum Geology, 163, 106715.

Robador Moreno, A., Zamorano Cáceres, M. (1999). Mapa Geológico de España. 1:50000, Hoja 212, Campo, IGME.

Roca, E., Sans, M., Koyi, H.A., 2006. Polyphase deformation of diapiric areas in models and in the Eastern Prebetics (Spain). AAPG Bull. 90, 115–136. http://dx.doi.org/10. 1306/07260504096.

Rodríguez-Pintó, A., Pueyo, E.L., Serra-Kiel, J., Barnolas, A., Samsó, J.M., Pocoví, A., 2013. The Ypresian–Lutetian boundary

895   in the Southwestern Pyrenean Basin; magnetostratigraphy from the San Pelegrín section. Palaeogeography, Palaeoclimatology, Palaeoecology, 370, 13-29.

Rodríguez-Pintó, A., Pueyo, E.L., Serra-Kiel, J., Samsó, J.M., Barnolas, A., Pocoví, A., 2012. Lutetian magnetostratigraphic calibration of larger foraminifera zonation (SBZ) in the Southern Pyrenees: The Isuela Section. Palaeogeography, Palaeoclimatology, Palaeoecology, 333-334, 107-120.

900   Rodríguez-Pintó, A., Serra-Kiel, J., Bernaola, G., Barnolas, A., Pueyo, E.L., Tosquella, J., Arbués, P., Scholger, R., 2022. The early/middle Eocene transition at the Ésera valley (South-Central Pyrenees): Implications in Shallow Benthic Zones (SBZ). Geologica Acta, 20.6, 1-25. DOI: 10.1344/GeologicaActa2022.20.6

Rowan, M. G. (2020). Salt- and shale-detached gravity-driven failure of continental margins. In N. Scarselli, J. Adam, D.

Rowan, M.G., Muñoz, J.A., Roca, E., Ferrer, O., Santolaria, P., Granado, P., Snidero, M. (2022). Linked detachment folds,

905   thrust faults, and salt diapirs: Observations and analog models. Journal of Structural Geology 155, 104509. https://doi.org/10.1016/j.jsg.2022.104509

Rowan, M.G., Vendeville, B.C., 2006. Foldbelts with early salt withdrawal and diapirism: physical model and examples from the northern Gulf of Mexico and the Flinders Ranges, Australia. Mar. Pet. Geol. 23 (9–10), 871–891.

Ruh, J. B., Kaus, B. J. P. and Burg, J. P. (2012). Numerical investigation of deformation mechanics in fold-and-thrust belts:

910   Influence of rheology of single and multiple décollements. Tectonics 31, TC3005, doi:10.1029/2011TC003047

Sánchez Rivera, R., Cruz Mercado, M.A., Reyes Tovar, E., López Céspedes, H.G., Peterson Rodríguez, R.H., Flores Zamora, J.C., León Ramírez, R., Barrera González, D., (2011). Tectonic evolution of the south Gulf salt province in the Gulf of Mexico. Gulf Coast Assoc. Geol. Soc. Trans. 61, 421–427.

Sans, M., Koyi, H.A., 2001, Modeling the role of erosion in diapir development in contractional settings. Geological Society

915   of America Memoir 193, p. 111-122

Santolaria, P., Casas-Sainz, A. M., Soto, R., Pinto, V., Casas, A, 2014. The Naval diapir (Southern Pyrenees): Geometry of a salt wall associated with thrusting at an oblique ramp. Tectonophysics, 637, 30-44.

Santolaria, P. (2015). Salt and thrust tectonics in the South Central Pyrenees. PhD thesis, University of Zaragoza, 327 pp.

Santolaria, P., Casas, A., Casas-Sainz, A. M. and Soto, R. (2016). Gravimetric modelling to assess salt tectonics in the western

920   end of the south Pyrenean central unit. Journal of the Geological Society 174 (2), 269-288. doi: 10.1144/jgs2016-027.

Santolaria, P., Ferrer, O., Rowan, M.G., Snidero, M., Carrera, N., Granado, P., Muñoz, J. A., Roca, E., Schneider, C.L., Piña, A., Zamora, G., 2021a. Influence of preexisting salt diapirs during thrust wedge evolution and secondary welding: insights from analog modeling. J. Struct. Geol. 149, 104374. https://doi.org/10.1016/j.jsg.2021.104374.

Santolaria, P., Granado, P., Carrera, N., Schneider, C.L., Ferrer, O., Snidero, M., Strauss, P., Pelz, K., Roca, E., Muñoz, J.A.,

925   2021b. From downbuilding to contractional reactivation of salt-sediment systems: Insights from analog modeling. Tectonophysics, 918, 229078, https://doi.org/10.1016/j.tecto.2021.229078.

Santolaria, P., Granado, P., Wilson, E. P., de Matteis, M., Ferrer, O., Strauss, P., et al. (2022). From salt-bearing rifted margins to fold-and-thrust belts. Insights from analog modeling and Northern Calcareous Alps case study. Tectonics, 41, e2022TC007503. https://doi.org/10.1029/2022TC007503

930   Saura, E., Vergés, J., Martín-Martín, J.D., Messager, G., Moragas, M., Razin, P., Grélaud, C., Joussiaume, R., Malaval, M., Homke, S., 2014. Syn-to post-rift diapirism and minibasin of the Central High Atlas (Morocco): The changing face of a mountain belt. Journal of the Geological Society, 171, 97-105.

Schaub, H., 1966. Ueber die Grossforaminiferen im Untereocaen von Campo Ober-Aragonien). Eclogae Geologicae Helvetiae, 59, 355-377.

935   Schaub, H., 1981. Nummulites et Assilines de la Téthys Paléogène. Taxinomie, phylogénese et biostratigraphie. Mémoires suisses de paléontologie, 104-105-106, 236pp, 97pl.

Schleder, Z., Tămaş, D.M., Krezsek, C., Arnberger, K., Tulucan, A. (2019). Salt tectonics in the Bend Zone segment of the Carpathian fold and thrust belt, Romania. International Journal of Earth Sciences 108, 1595–1614

Schlumberger, C. (1905). Deuxième note sur les Miliolidées trématophorées. Bulletin de la Société géologique de France.

940   (série 4) 5 (2): 115-134

Séguret, M. (1972). Etude tectonique de nappes et series decollés de la partie central du versant sud des Pyrenées. Caractére sedymentaire rôle de la compression et de la gravité. Tesis doctoral, Univ. de Montpellier, 155 pp.

Serra-Kiel, J., Hottinger, L., Caus, E., Ferràndez, C., Jauhri, A.K., Less, G., Pavlovec, R., Pignatti, J., Samsó, J.M., Schaub, H., Sirel, E., Strougo, A., Tosquella, J., Zakrevskaya, E., 1998. Larger foraminiferal biostratigraphy of the Tethyan Paleocene

945   and Eocene. Bulletin de la Société géologique de France, 169(2), 281-299.

Snidero, Carrera, M. N., Mencos, J., Butillé, M., Granado, P., Tavani, S., Lopez-Mir, B., Sàbat, F., Muñoz, J. A., 2020. Diapir kinematics in a multi-layer salt system from the eastern Persian Gulf, Marine and Petroleum Geology, 117, 104402, ISSN 0264-8172.

Soto, R., Casas, A. M., Storti, F. and Faccenna, C. (2002). Role of lateral thickness variations on the development of oblique

950   structures at the western end of the South Pyrenean Central Unit, Tectonophysics 350, 215-235.

Stefanescu, M., Dicea, O., Tari, G. (2000) Influence of extension and compression on salt diapirism in its type area, East Carpathian Bend area, Romania. In: Vendeville BC, Mart Y, Vigneresse JL (eds) Salt, shale and igneous diapirs in and around Europe. Geological Society, London, pp 131–147. https ://doi.org/10.1144/GSL.SP.1999.174.01.08.

Stewart, S. A. (1999). Geometry of thin-skinned tectonic systems in relation to detachment layer thickness in sedimentary
955   basins. Tectonics 18, 719-732.

Storti, F., McClay, K.R. 1995. Influence of syntectonic sedimentation on thrust wedges in analogue models. Geology 23 (11): 999–1002. doi: https://doi.org/10.1130/0091-7613(1995)023<0999:IOSSOT>2.3.CO;2

Strauss, P., Granado, P., Muñoz, J.A., Böhm, K., Schuster, R., (2023). The Northern Calcareous Alps revisited: Formation of a hyperextended margin and mantle exhumation in the Northern Calcareous Alps sector of the Neo-Tethys (Eastern Alps,
960   Austria). Earth-Science Reviews, 243, 104488, https://doi.org/10.1016/j.earscirev.2023.104488

Tavani, S., Storti, F., Fernández, O., Muñoz, J.A., Salvini, F. (2006). 3-D deformation pattern analysis and evolution of the Añisclo anticline, southern Pyrenees. Journal of Structural Geology 28 (4), 695-712.

Teixell, A. (1996). The Ansó transect of the southern Pyrenees: basement and cover thrust geometries. J. Geol. Soc. London 153, 301-310.

965   Teixell, A., García Senz, J., and Ramirez Merino, J. I., (1994a). Mapa Geológico de España. 1:50000, Hoja 288, Fonz, IGME. and Barnolas, A. (1995). Significado de la discordancia de Mediano en relación con las estructuras adyacentes (Pirineo central). Geogaceta 17, 186-189.

Teixell, A., Zamorano, M. and Ramirez Merino, J. I., (1994b). Mapa Geológico de España. 1:50000, Hoja 250, Graus, IGME. Teixell, A. and Barnolas, A. (1995). Significado de la discordancia de Mediano en relación con las estructuras adyacentes
970   (Pirineo central). Geogaceta 17, 186-189.

Teixell, A., Barnolas, A., Rosales, I., Arboleya, M.L., 2017. Structural and facies architecture of a diapir-related carbonate minibasin (lower and middle Jurassic, High Atlas, Morocco). Marine and Petroleum Geology, 81, 334-360.

Teixell, A., Labaume, P., Lagabrielle, Y., 2016. The crustal evolution of the west-central Pyrenees revisited: inferences from a new kinematic scenario. Compt. Rendus Geosci. 348, 257–267. https://doi.org/10.1016/j.crte.2015.10.010.

975   Teixell, A., Labaume, P., Ayarza, P., Espurt, N., de Saint Blanquat, M., Lagabrielle, Y. (2018). Crustal structure and evolution of the Pyrenean-Cantabrian belt_ A review and new interpretations from recent concepts and data. Tectonophysics 724-725, 146–170. http://doi.org/10.1016/j.tecto.2018.01.009

Vakalas, I.; Kokkalas, S.; Konstantopoulos, P.; Tzimeas, C.; Kampolis, I.; Tsiglifi, H.; Pérez-Martin, R.; Hernandez-Jiménez, P.; Pita-Gutierrez, J.P. Implications of Salt Diapirism in Syn-Depositional Architecture of a Carbonate Margin-to-Edge
980   Transition: An Example from Plataria Syncline, Ionian Zone, NW Greece. Appl. Sci. 2023, 13, 7043. https://doi.org/10.3390/app13127043

Velaj, T. Evaporites in Albania and their impact on the thrusting processes. Carbonates Evaporites 2002, 17, 68–78.

Vendeville, B. C. and Jackson, M. P. A. (1992). The rise of diapirs during thin-skinned extension. Marine and Petroleum Geology 9, 331–353.

985 Vendeville, B.C., Nilsen, K.T., 1995. Episodic growth of salt diapirs driven by horizontal shortening. In: Travis, C.J., Harrison, H., Hudec, M.R., Vendeville, B.C., Peel, F.J., Perkins, B.F. (Eds.), Salt, Sediment, and Hydrocarbons. SEPM Gulf Coast Section 16th Annual Research Foundation Conference, pp. 285–295.

Wiltschko, D.V., and Chapple, W.M., 1977. Flow of weak rocks in Appalachian Plateau folds: American Association of Petroleum Geologists Bulletin,v. 61, p. 653–670.